THE POLE-ZERO ANALOGUE COMPUTER

A Thesis

Presented to

the Faculty of Graduate Studies and Research

The University of Manitoba

In Partial Fulfillment

of the Requirements for the Degree

Master of Science

by

Dennis F. Johnson

November 1961

ABSTRACT

This thesis deals with the description and testing of a special-purpose computer, called the pole-zero analogue computer. This machine is capable of solving network functions and can be used to plot Nichols loci, root loci, and equipotential lines about line charges. In addition facilities are included to aid in the approximation of response functions by positioning poles and zeros.

PREFACE

The history of the pole-zero analogue computer dates from the early 1950's when the basic design was developed by Ragazzini and Reynolds (Ra 1). An improved version of their "Complex-Plane Scanner", as it was called, was constructed by Kranc, Mauzey, and Wuorinen (Kr 1).

Further development was begun at the University of Manitoba in 1956 with the construction of a machine similar to the Complex-Plane Scanner by Valstyn (Va 1), and at a later date Wagerer (Wa 1) began the development of a phase measuring technique called the "horizontal-sweep method". Subsequently, an "error-measuring unit" (Hi 1) and an "antilogarithmic-unit" (Wn 1) were developed by Hill and Woon-Sam respectively.

This thesis contains an account of the completed pole-zero machine, including a description of a comparator useful for plotting root loci. Many of the original units have been extensively modified or redesigned, and only the final versions are described.

The entire project has been made possible through financial support by the National Research Council of Canada.

The author wishes to acknowledge the assistance received from Professor R. A. Johnson, Mr. B. Bigelow, Mr. R. J. Burns, and Mr. R. J. Tarry.

TABLE OF CONTENTS

CHAPTER PAGE

LIST OF TABLES

LIST OF FIGURES

FIGURE PAGE

FIGURE PAGE

CHAPTER I

THEORY

In the fields of circuit theory and control systems it is often necessary to evaluate network functions of the form

$$F(s) = \frac{(s - z_1)(s - z_2)\cdots\cdots\cdots(s - z_n)}{(s - p_1)(s - p_2)\cdots\cdots\cdots(s - p_m)} \qquad (1)$$

where s is a complex variable and the z's and p's are complex numbers. Several practical approaches to obtaining an analogue of such a function are in existence, namely, the electrolytic tank (Bo 1) and the conducting sheet (Ha 1; Br 1), both of which are based on the "potential analogue" (Se 1). However, the all-electronic analogue to be described offers a variety of advantages over the previous methods. These are:

1. Ease of positioning singularities.
2. More rapid calculation of F(s).
3. A linear frequency scale.
4. Greater versatility.

I. THE ELECTRONIC ANALOGUE

An electronic analogue of equation (1) is suggested by an examination of its representation in the complex plane,

or more particularly, the representation of a general term such as $(s - p_1)$, where

$$s = \sigma + jw \tag{2}$$

and

$$p_1 = a + jb \tag{3}$$

The location of point p_1 in the complex plane is determined by its real and imaginary parts as indicated in Figure 1. Also, p_1 may be considered to lie at the terminus of two mutually

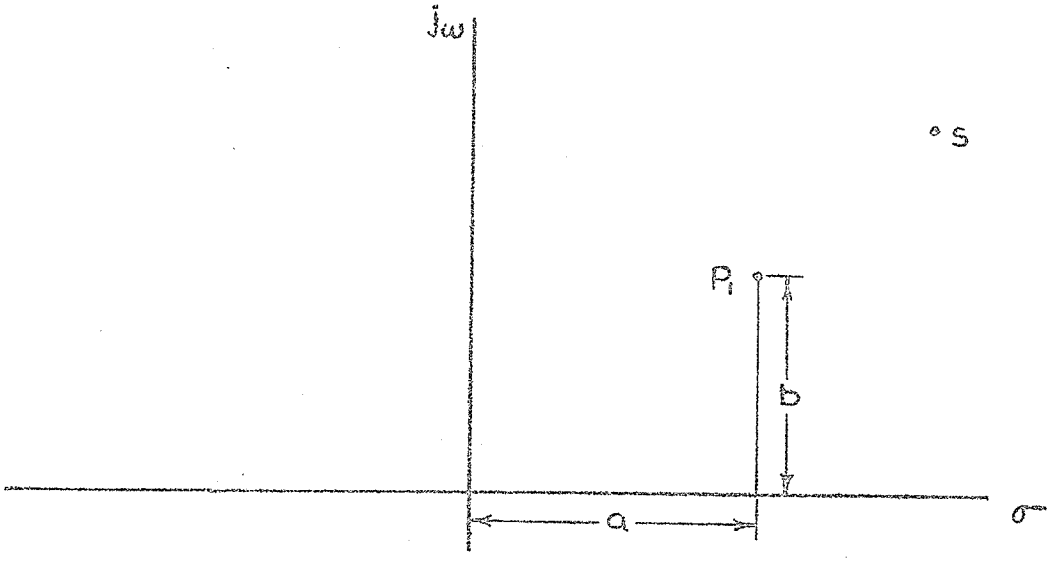

Figure 1. Location of p_1 in the s plane.

perpendicular vectors, $\overline{a}$ and $\overline{b}$, which lie in the σ and jw directions respectively, as shown in Figure 2. Similarly s consists of vectors $\overline{\sigma}$ and $\overline{w}$.

Thus,

$$s = \sigma + jw \qquad \text{or} \qquad \overline{s} = \overline{\sigma} + \overline{w}$$

and

$$p_1 = a + jb \qquad \text{or} \qquad \overline{p_1} = \overline{a} + \overline{b}$$

For a term such as $(s - p_1)$ we have

$$(s - p_1) = (\sigma + jw) - (a + jb)$$

$$= (\sigma - a) + j(w - b)$$

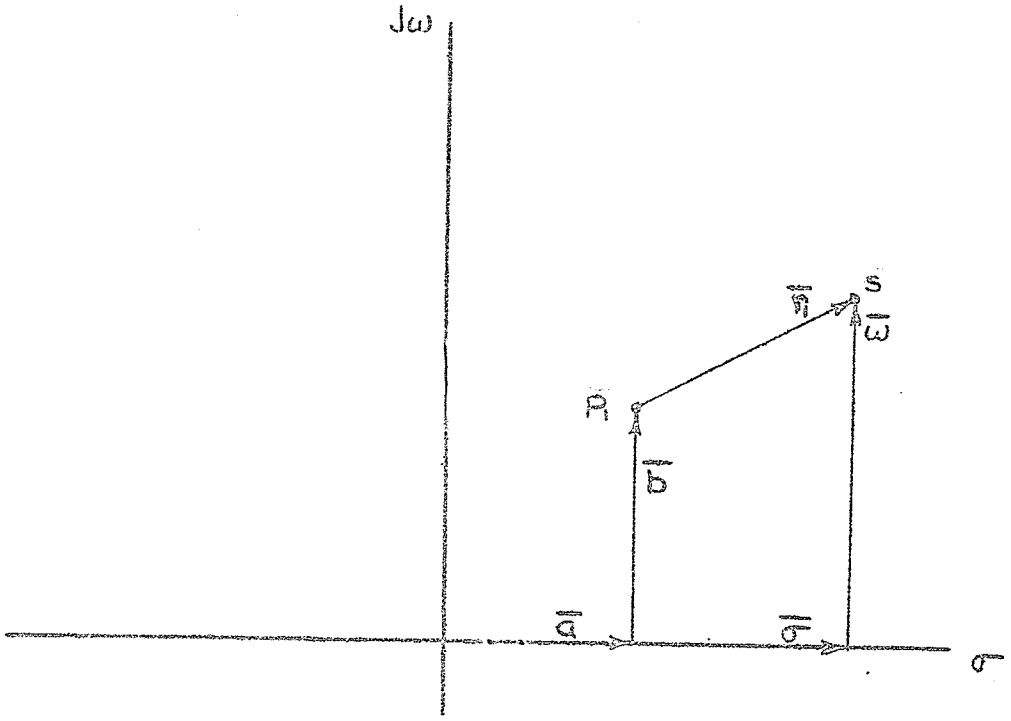

Figure 2. Vector representation of p_1 and s.

Applying Euler's Theorem,

$$(s - p_1) = r_1 e^{j\theta}$$

where

$$r_1 = \sqrt{(\sigma - a)^2 + (w - b)^2}$$

and

$$\theta = \text{Arctan } \frac{(w - b)}{(\sigma - a)}$$

The term, $r_1 e^{j\theta}$, may also be interpreted as a vector (as shown in Figure 2), obtained by vector subtraction. That is to say,

$$r_1 e^{j\theta} = \overline{s} - \overline{p_1} = (\overline{\sigma} + \overline{w}) - (\overline{a} + \overline{b})$$

It has thus been shown that p_1, s, and $(s - p_1)$ may be depicted by vectors. However, they could just as easily be represented by phasors, since the two are equivalent providing constant phase relationships are maintained between phasors.

This observation was implemented by Ragazzini and Reynolds (Ra 1) in the design of a computer which utilized voltage phasors as analogues of the terms in equation (1). A point such as p_1 may be represented by the addition of two mutually perpendicular phasors of appropriate magnitude, as indicated in Figure 3. A voltage, Vp, of the form

$$Vp \angle \alpha = Va \angle 0^\circ + Vb \angle 90^\circ \qquad (4)$$

is obtained. Similarly,

$$Vs \angle \beta = V\sigma \angle 0^\circ + Vw \angle 90^\circ \qquad (5)$$

By subtracting (4) from (5) a phasor is obtained which corresponds to $(s - p_1)$.

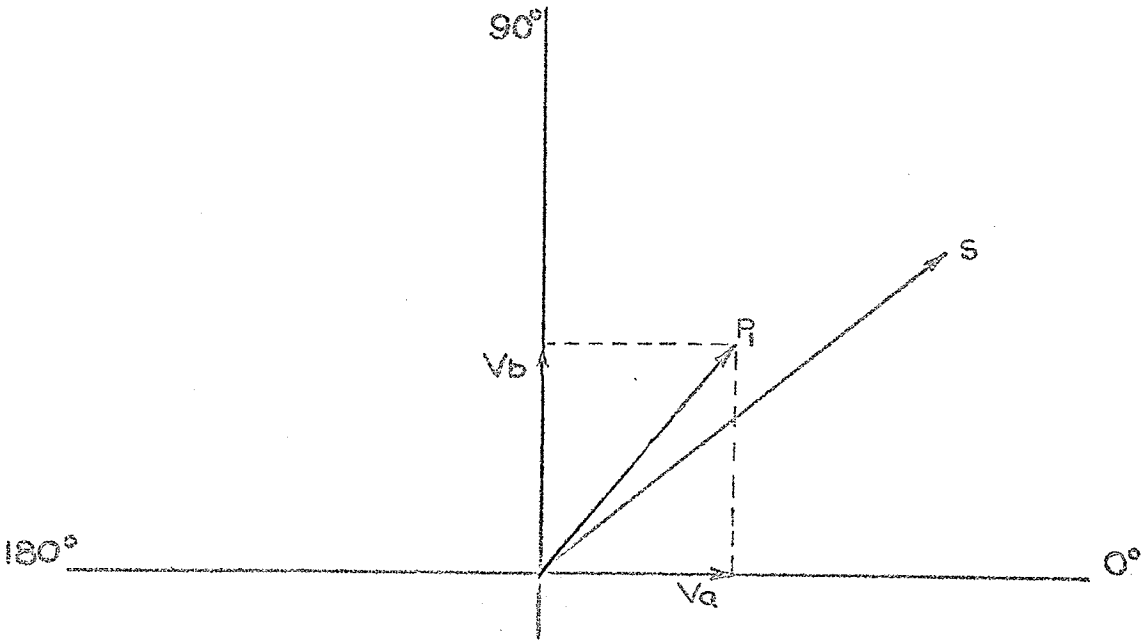

Figure 3. Phasor representation of p_1 and s.

II. EVALUATION OF THE MAGNITUDE OF F(s)

Once analogues of the terms, $(s - p_1)$, $(s - p_2)$, etcetera are obtained, two approaches are available for determining the magnitude of F(s). The direct course involves taking the product of the numerator factors of F(s) and dividing the result by the product of the denominator

factors. That is to say,

$$|F(s)| = \frac{\prod_{i=1}^{n} |s - z_i|}{\prod_{k=1}^{m} |s - p_k|} \tag{6}$$

The indirect approach may be expressed mathematically as follows. By equation (1)

$$F(s) = \frac{(s - z_1)(s - z_2)\cdots\cdots\cdots(s - z_n)}{(s - p_1)(s - p_2)\cdots\cdots\cdots(s - p_m)} \tag{7}$$

Taking logarithms,

$$\ln |F(s)| = \sum_{i=1}^{n} \ln|s - z_i| - \sum_{k=1}^{m} \ln|s - p_k| \tag{8}$$

from which

$$|F(s)| = \text{Antilog } \ln|F(s)| \tag{9}$$

From an electronics viewpoint, it is more expedient to obtain $|F(s)|$ by the logarithmic method, utilizing equations (8) and (9). (This is the technique used by Ragazzini and Reynolds (Ra 1) and later by Kranc, Mauzey, and Wuorinen (Kr 1; Bi 1) in the construction of two "complex-plane scanners".) In addition, the availability of $\ln|F(s)|$ is

particularly useful in connection with the plotting of Nichols Loci and Bode Diagrams.

III. EVALUATION OF THE ARGUMENT OF F(s)

The most obvious method of computing the argument of F(s) is to measure the phase angle of each phasor, representing a factor such as $(s - p_1)$, with respect to a reference phasor, using phasemeters. Then

$$\text{Arg } F(s) = \sum_{i=1}^{n} \text{Arg } (s - z_i) - \sum_{k=1}^{m} \text{Arg } (s - p_k) \qquad (10)$$

However, this method requires a separate phasemeter for each factor in F(s). Consequently a second method, called the horizontal-sweep method (Wa 1), has been investigated. This method is essentially an extension of techniques used by Ragazzini and Reynolds (Ra 1) to measure the phase slope of F(s). It is derived from complex-variable theory.

Since F(s) is a function of a complex variable, it may be shown that

$$\ln F(s) = \ln|F(s)| + j \text{ Arg } F(s)$$

At all points where ln F(s) is analytic the Cauchy-Riemann conditions give

$$\frac{\partial \ln|F(s)|}{\partial \sigma} = \frac{\partial \text{ Arg } F(s)}{\partial w} \equiv \frac{\partial \psi}{\partial w}$$

where $\frac{\partial \phi}{\partial w}$ is called the phase slope. From equation (2)

$$s = \sigma + jw$$

If the real part, σ, of s is allowed to vary (sweep) from σ_1 to σ_2, while w remains constant, the derivative of $\ln|F(s)|$ with respect to σ yields the phase slope over the range

$$s = (\sigma_1 + jw_1) \quad \text{to} \quad s = (\sigma_2 + jw_1)$$

This is illustrated in Figure 4.

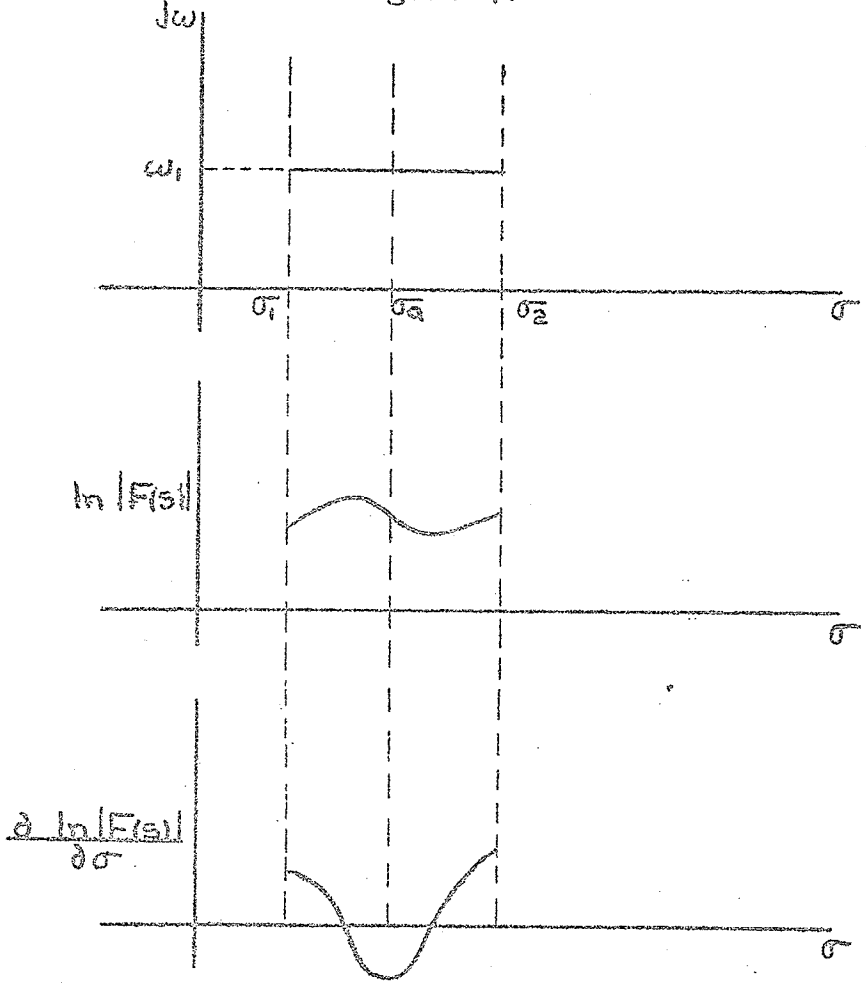

Figure 4. Effect of changing σ from σ_1 to σ_2 with w constant.

A sample of $\frac{\partial \ln |F(s)|}{\partial \sigma}$ taken at $\sigma = \sigma_a$ is the value of the phase slope, $\frac{\partial \phi}{\partial w}$, at the point $s = \sigma_a + jw_1$. Repetition of the σ sweep for a second value of w ($w = w_2$), accompanied by differentiation and sampling of $\ln|F(s)|$ at $\sigma = \sigma_a$, yields a second value of phase slope. By rapid repetition of this process a large number of samples of phase slope may be obtained along a line of constant σ. Integration of these samples with respect to w, gives the phase function along the line of constant σ ($\sigma = \sigma_a$). Of particular interest to the circuit designer is the case where $\sigma_a = 0$. For the above process this gives the phase of the steady state response function as s varies from (0 + j0) to (0 + jw) where w is some large frequency.

Considering the electronic computation; differentiation and integration are only possible with respect to time. However, this difficulty may be easily overcome by making the magnitude of the phasors representing σ and w linear functions of time. This is accomplished by amplitude modulation of the appropriate phasors so that

$$V\sigma(t) \angle 0^\circ = Vx\,t \angle 0^\circ + Vk \angle 0^\circ$$

and

$$Vw(t) \angle 90^\circ = Vy\,t \angle 90^\circ$$

In practice, the jw axis must be scanned in steps (w remaining constant between steps) so that in order to approximate $Va(t) \angle 90^\circ = Vx\ t \angle 90^\circ$, the steps must be: (1) of equal amplitude and duration, and (2) small with respect to the total range of w to be covered.

During the time that the phasor representing w remains constant, the phasor representing σ is amplitude modulated such that it starts out at $V\sigma \angle 180^\circ$ and decreases linearly (at a constant rate) to zero and then increases in the same manner to $V\sigma \angle 0^\circ$ as shown in Figure 5.

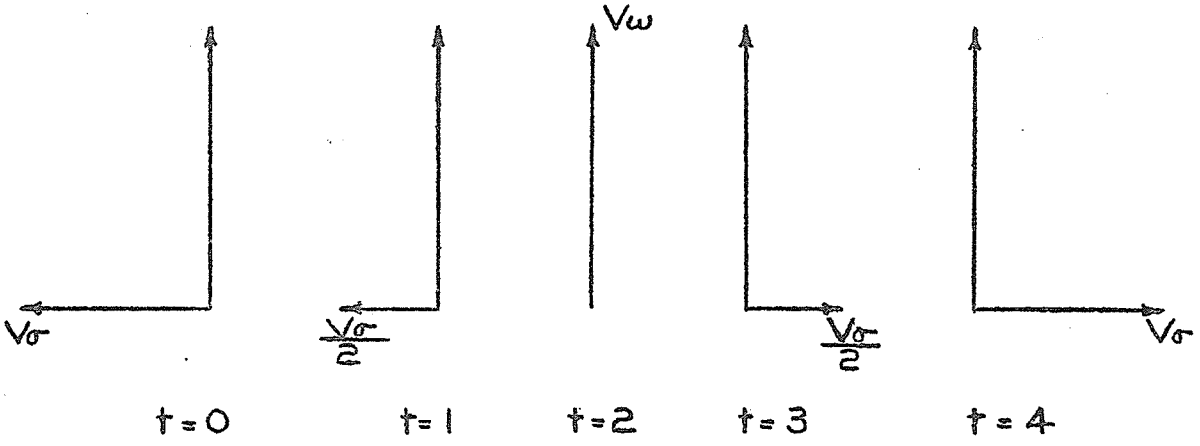

Figure 5. The horizontal sweep.

The derivative of $\ln |F(s)|$ is sampled when $\sigma = 0$. Upon completion of the horizontal sweep at $t = 4$, w jumps by a discrete amount and the sweeping process is again initiated.

This yields distinct values of phase slope at equal time intervals, which may be used to generate a continuous function using electronic data-reconstruction techniques. Integration of this function gives the argument of F(s).

If integration starts from w = 0 the constant of integration will be n $\frac{\pi}{2}$, its exact value being obvious by inspection of F(s).

If ln $|F(s)|$ is sampled at the same time, the values thus obtained may be reconstructed to form a smooth curve of ln $|F(s)|$ versus w.

CHAPTER II

THE POLE-ZERO MACHINE

I. THE GENERAL SYSTEM

The pole-zero analogue computer to be described was constructed to simulate singularities in the complex plane and to perform the operations required to evaluate F(s). Provision has been made for the independent variable, s, to automatically traverse two different paths in the s plane: (1) a repetitive path along the jw axis, and (2) a repetitive path in the jw direction at equally spaced intervals of σ, covering the entire plane. These sweeps will be referred to as the jw sweep and the plan sweep respectively. In addition, s may be positioned manually. Several ancillary units provide facilities for evaluating errors, plotting root loci, and determining the antilog of $\ln|F(s)|$.

The overall block diagram of the pole-zero machine is displayed in Figure 6. A stable oscillator generates a 1600-cps sinusoidal carrier which is converted to four reference voltages (phasors): $6\angle 0^\circ$, $6\angle 90^\circ$, $6\angle 180^\circ$, and $6\angle 270^\circ$. These reference phasors are supplied to twelve separate factor synthesizers, where the appropriate phasors and phasor magnitudes are combined with the s phasor to represent one factor (either a pole or a zero) of F(s). In addition, the reference

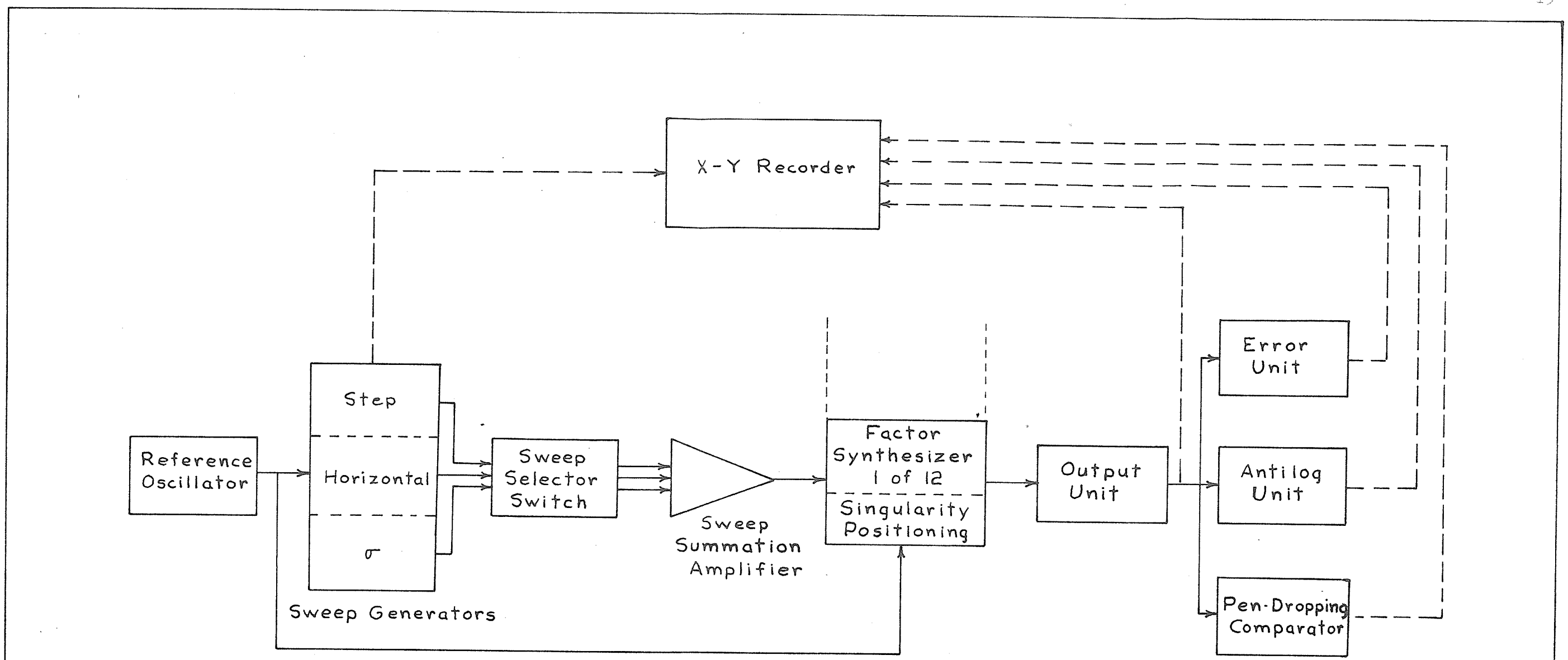

Figure 6. General block diagram of the pole-zero machine

voltages are fed to the sweep generators where they are amplitude modulated to represent the variable s. Depending on the desired mode of operation, that is, jw sweep, plan sweep, or manual sweep, the appropriate output(s) of the sweep generators are switch selected and applied to a sweep-summation amplifier which in turn supplies the sweep output to all the factor synthesizers simultaneously. Each factor synthesizer handles one singularity, and its output is a slowly varying (with s) d-c voltage (positive for zeros and negative for poles) which represents one factor such as $\ln |s - p_1|$. Finally the output unit sums the output of each channel to yield $\ln |F(s)|$. In addition, the output unit embodies circuits for determining the phase slope and phase of F(s).

The functions of the remaining blocks are self explanatory, but details of their operation will be discussed in a subsequent section entitled, "Ancillary Units".

A description of the various operating modes will be preceded by a more detailed examination of the units common to all modes of operation, namely, the reference oscillator, the factor synthesizers, and part of the output unit.

The Reference Oscillator

The reference oscillator, whose self explanatory block diagram appears in Figure 7, generates the system reference phasors. Standard circuitry is used throughout,

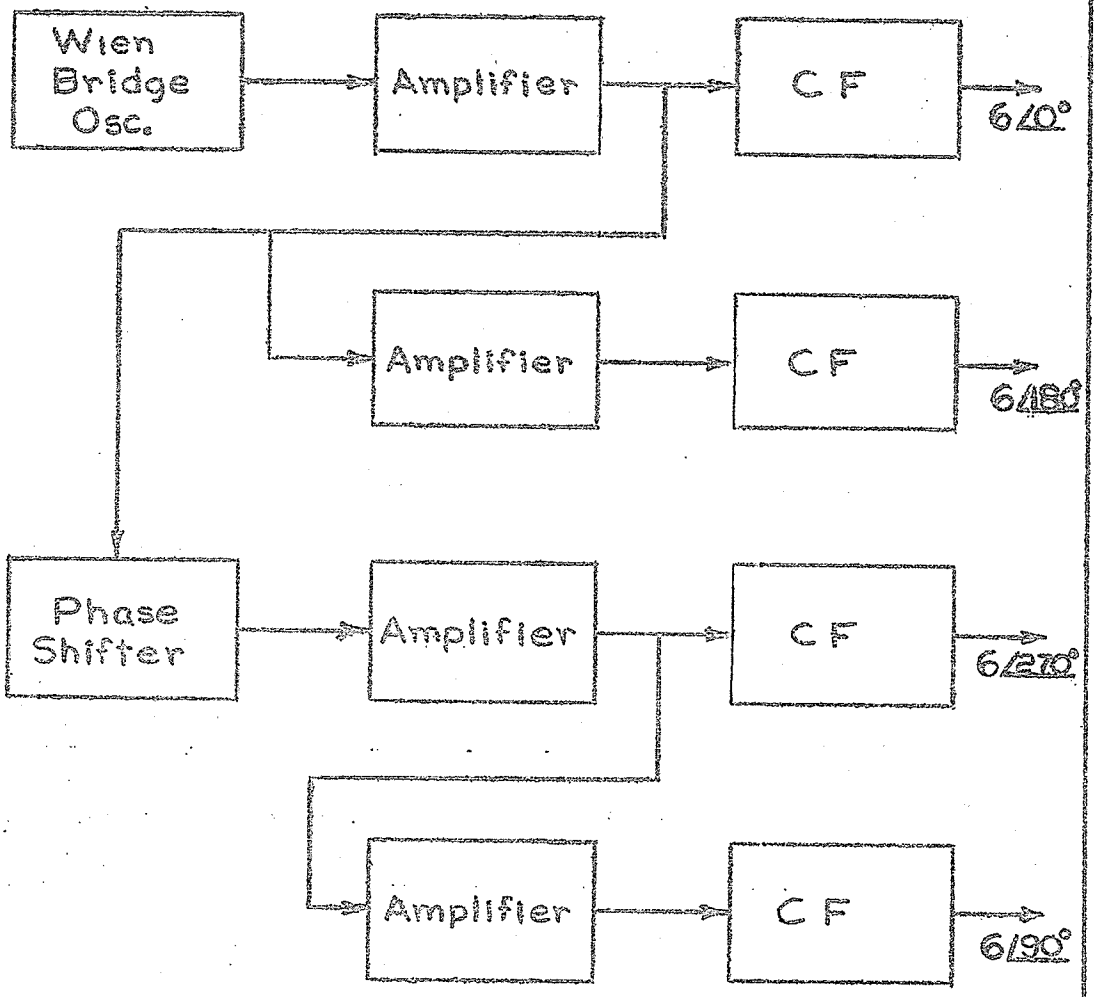

Figure 7. Reference oscillator.

while high quality components and extensive shielding ensure stable operation.

It may be noted that the adjustment of the four reference phasors is quite critical with regard to the accuracy of the computer. However, methods are available which permit very precise adjustment; these methods are discussed in Appendix II.

The Factor Synthesizer

Details of a single synthesizer are shown in Figure 8. Switches select the reference voltages (phasors) required to represent the real and imaginary parts of a singularity, while precision, ten-turn potentiometers are set so that the appropriate amplitudes of the real and imaginary carriers are applied to the summing amplifier. The -s phasor from the sweep amplifier is also applied to the summing amplifier whose output is a phasor $A(s - p_1)$, where A is the gain of the summing amplifier. This voltage is then applied to a logarithmic attenuator whose output is given by

$$e_{out} = K \ln e_{in} + C$$

for 0.1 volts $< e_{in} <$ 100 volts. The logarithmic attenuator output is thus a wave whose peak amplitude is given by

$$Ep = K \ln |A(s - p_1)| + C$$

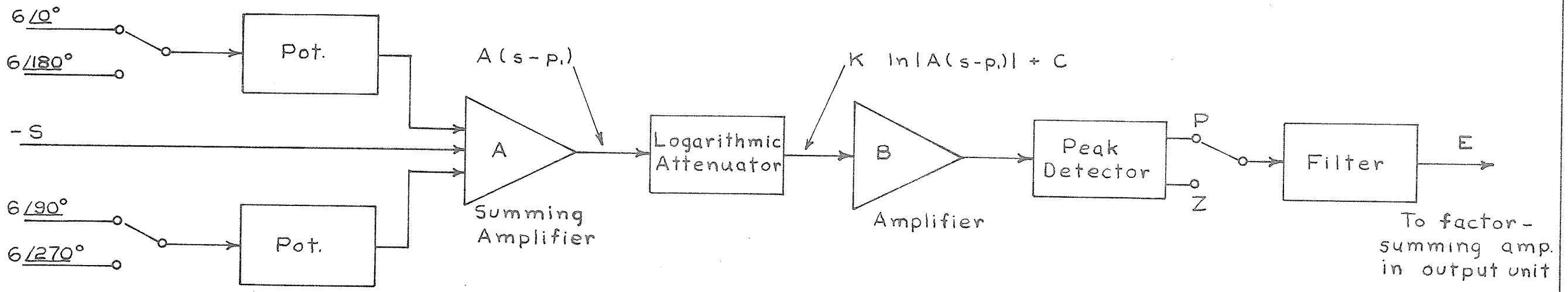

Singularity $(s - p_1) = (s - a - jb)$

Figure 8. The factor synthesizer (1 of 12).

Amplification of this low-level signal is followed by variable-polarity peak detection (positive for zeros, negative for poles), while smoothing is accomplished by a low-pass, R-C filter in cascade with a twin-T filter having a 40 dbv notch at the ripple frequency. The output voltage, E, is given by

$$E = BK \ln \left| A(s - p_1) \right| + BC + D$$

where B is the gain between attenuator output and filter output, and D is a shift in d-c level due to the Edison Effect in the peak-detector diodes.

The Output Unit

That part of the output unit common to all modes of operation is a summing amplifier which sums the synthesizer outputs to give a d-c voltage of the form

$$M \ln A\left|F(s)\right| + N \qquad (11)$$

where A, M, and N, are machine constants.

II. SWEEP MODES

As was previously mentioned, several sweep configurations are available. The following section gives a detailed account of sweep generating methods plus the operating details of the output unit.

The jw Sweep

By allowing s to vary in small steps along the jw axis, while the real part of s is swept horizontally across the jw axis during the interval between steps (as shown in Figure 9), it is possible to investigate the frequency response of any system represented by F(s).

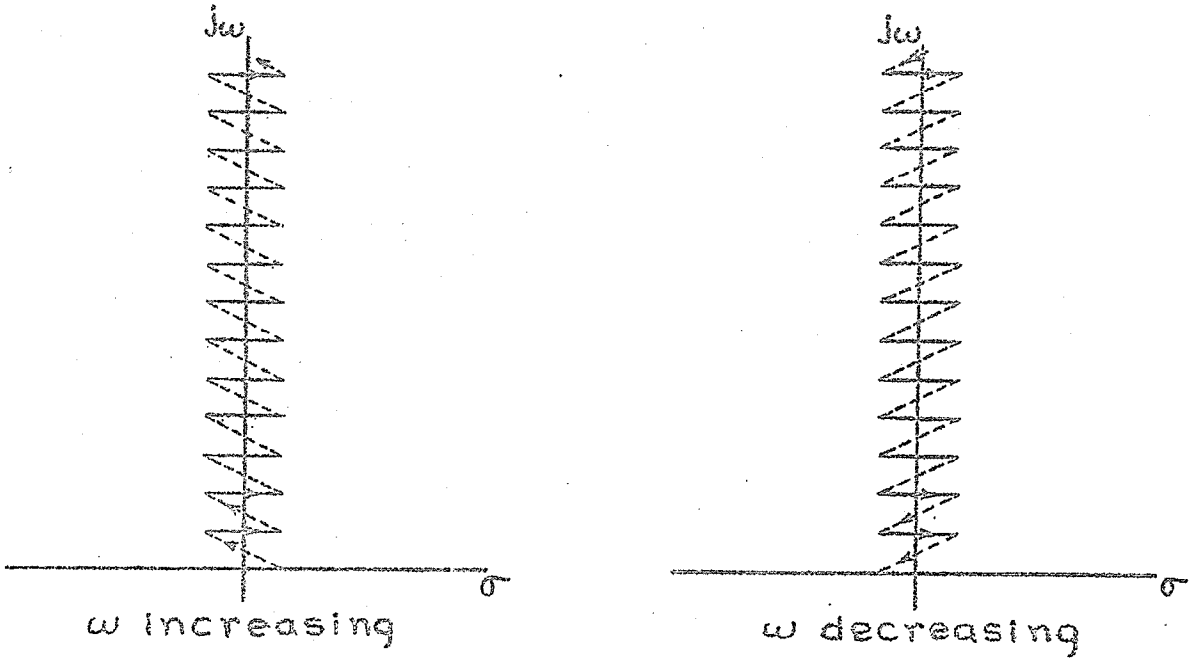

Figure 9. Path of the jw sweep.

This jw sweep is created by staircase modulation of the carrier voltage $6\angle 90^\circ$, to which is added a horizontal sweep consisting of double sawtooth modulation of the carriers $6\angle 180^\circ$ and $6\angle 0^\circ$. This type of modulation is illustrated in Figure 10.

A block diagram of the jw-sweep generator is shown in Figure 11, the upper chains of blocks being used to create the step portion of the sweep, while the lower chain generates the horizontal sweep.

Beginning with the synchronizing chain (third row), a 1600-cps sine wave from the reference oscillator is applied

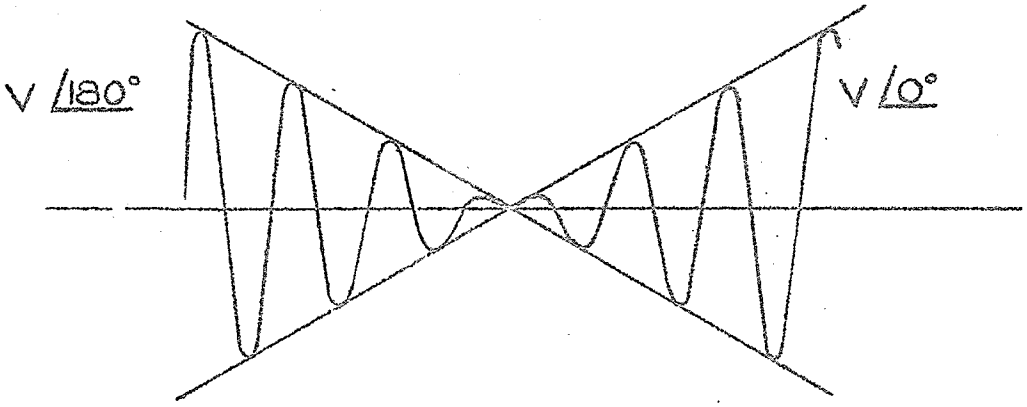

Figure 10. Double-sawtooth modulation.

to an astable multivibrator which divides the input by sixteen. A further division by two, in a second astable multivibrator, yields trigger pulses with a pulse repetition frequency of 50 pulses per second. These pulses are differentiated, amplified, and applied to a monostable multivibrator whose one millisecond-duration output pulses control a six-diode gate. Functioning as a nearly perfect switch, the six-diode gate applies the output of a cathode follower to a zero-order hold circuit every 20 milliseconds, for a period of one millisecond. Since the cathode follower output is a triangular waveform, having a period of 4.8 or 30 seconds, the output of the hold circuit is a staircase waveform (Figure 12d) having 50 steps per second, the step height being determined by the slope of the cathode-follower output. This staircase waveform is then used to modulate the 6 $\angle 90^{\circ}$ carrier to obtain the step portion of the sweep. (Figure 12c.)

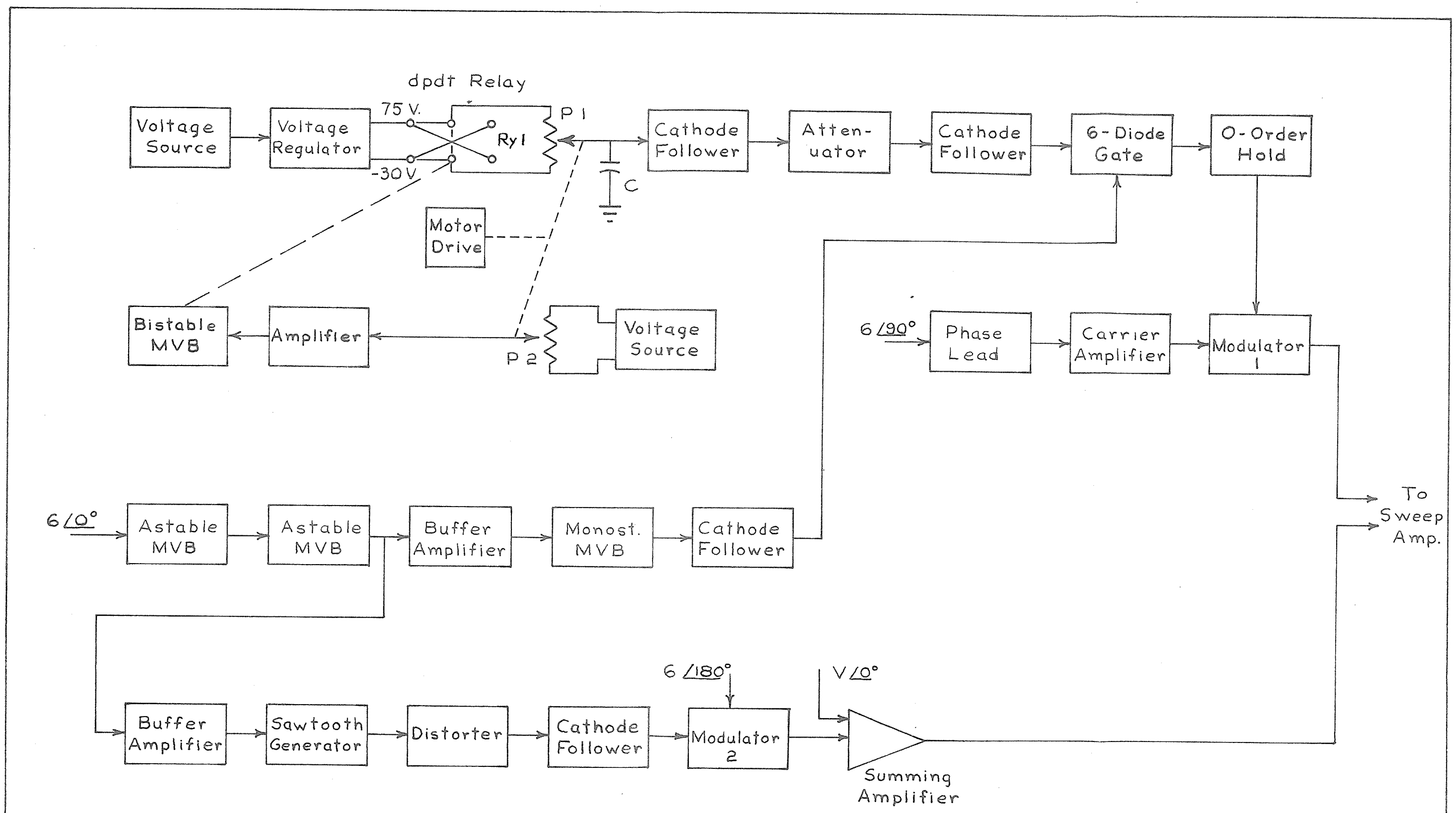

Figure 11. Block diagram of the jω-sweep unit.

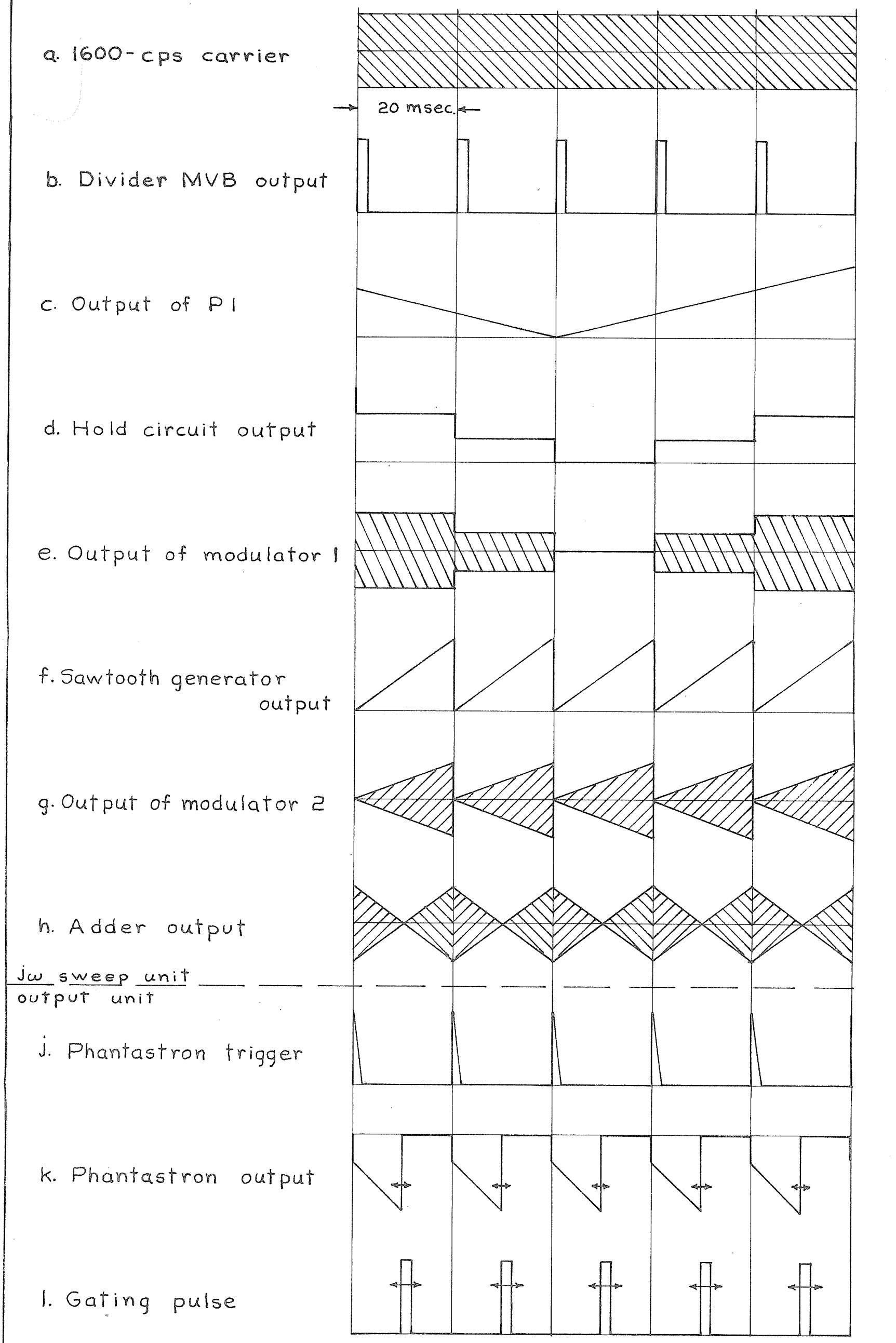

Figure 12. Timing chart.

The triangular waveform previously mentioned is generated by a motor-driven, continuous-rotation potentiometer having a reversible-polarity input as shown in Figure 11. A second potentiometer, coupled to the same shaft, provides pulses which control the polarity-reversing relay (Ry 1). The sequence of operations is as follows. Considering Ry 1 to be in the position shown, the output of potentiometer number one (P 1) is a rising ramp voltage. At the same time, the output of potentiometer number two (P 2) is a rising ramp which falls to zero just as the wiper of P 1 enters the dead zone between the ends of the resistance wire. This negative going pulse, after amplification and shaping, flips a symmetrically-triggered, bistable multivibrator with the coil of Ry 1 in one plate circuit. The switching of this relay reverses the polarity of the voltage applied to P 1, and the wiper, having just left the top end at +75 volts, comes in contact with the lower end which has just been switched to +75 volts. The potentiometer output then continues as a falling ramp. Again the output of P 2 is a rising ramp which will fall suddenly to zero after one rotation, once more initiating the switching process.

Capacitor C is required to prevent the output of P 1 from falling to zero, while the wiper arm is not in contact with the potentiometer resistance wire.

It may be noted that the output of the hold circuit is analagous to the variable jw, and, as such, may be used to drive one axis of the output recorder when plotting $\ln|F(s)|$, $|F(s)|$, or Arg F(s) against w.

The horizontal sweep is generated by the lower chain of blocks (of Figure 11) at a rate of 50 sweeps per second, synchronized with the steps of the previous portion of the jw sweep. Trigger pulses derived from the output of the second divider multivibrator are used to control a sawtooth generator which produces the horizontal-sweep modulation envelope. Amplification of the sawtooth by a nonlinear amplifier (distorter) compensates for nonlinearities of the balanced modulator used to produce the waveform shown in Figure 12g. To this waveform, oriented at 180 degrees, a constant voltage of $V\angle 0^{\circ}$ is added by means of a summing amplifier. The result is the double sawtooth waveform of Figure 12h, which represents a negative σ_1, falling at a constant rate to zero and then increasing to a positive σ_1, at which time the cycle is repeated with σ changing suddenly from σ_1 to $-\sigma_1$.

Finally, by addition in the sweep summation amplifier, the step and horizontal sweeps are combined to form the complete jw sweep.

The Output Unit

It has been shown that phase information may be extracted from $\ln|F(s)|$, using the horizontal sweep method, by

sampling $\frac{\partial \ln |F(s)|}{\partial t}$ when $\sigma = 0$. The circuits which perform this operation as well as others essential to the determination of Arg F(s) are shown in block diagram form in Figure 13. The output of the factor-summing amplifier, $\ln |F(s)|$, is applied to a low pass filter having a constant phase-slope characteristic over the pass band, and a cutoff frequency of 160-cps. This reduces the 1600-cps ripple in $\ln |F(s)|$ to a tolerable level. A differentiator, utilizing an operational amplifier, is used to differentiate $\ln |F(s)|$, and the derivative is then sampled by means of a six-diode gate and held in a zero-order hold circuit. The sampling period is controlled by a monostable multivibrator whose two-millisecond gating pulse allows the gate to conduct. This multivibrator receives a delayed trigger pulse via an amplifier and phantastron-delay circuit from the sawtooth generator which controls the horizontal sweep. The phantastron delay (about fifteen milliseconds) is adjusted so that the gate conducts prior to, and stops conducting when, $\sigma = 0$. (The point $\sigma = 0$ corresponds to the null in the waveform of Figure 12h). In practice, the gate stops conducting several milliseconds after $\sigma = 0$ to allow for the phase delay of the smoothing filters.

The sampled data available from the six-diode gate is converted to a smooth function by passing the output of the hold circuit through a low-pass filter consisting of a Butterworth filter in cascade with a twin-T filter. (This filter configuration has a cutoff frequency of 10-cps and an attenuation

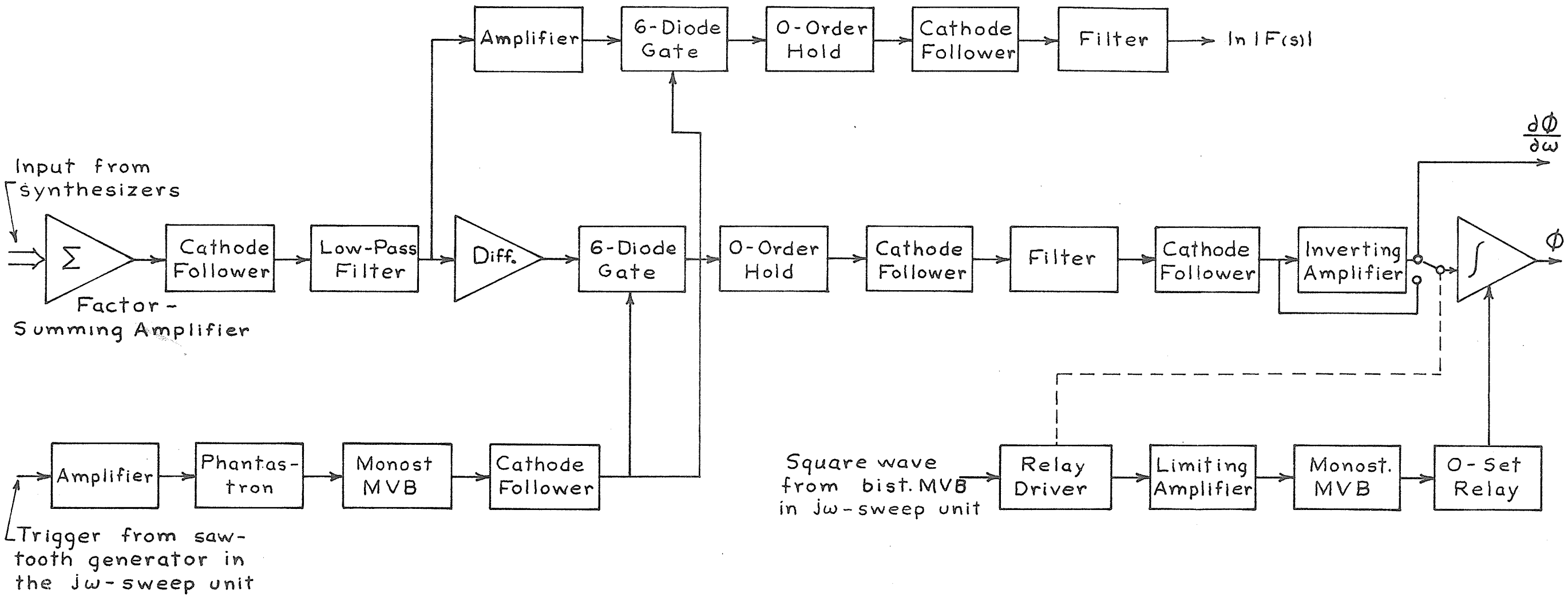

Figure 13. Block diagram of the output unit.

of 60 dbv at 50-cps.) The filter output, which constitutes the phase slope, is then integrated to yield Arg F(s). An inverting amplifier and relay preceding the integrator are used to reverse the polarity of the phase slope to allow integration while w is decreasing. This polarity-reversing relay is located in the cathode circuit of an amplifier which receives a square wave from the bistable multivibrator in the jw-sweep unit. Thus, the position of the relay is determined by sign $\frac{\partial w}{\partial t}$. Finally, the square-wave output from the plate of the relay driver is differentiated and limited so that it triggers a monostable multivibrator each time sign $\frac{\partial w}{\partial t}$ changes from negative to positive. This drives another relay which momentarily shorts the phase-slope integrator capacitor, thus preventing any integration errors from accumulating. Another sampling chain of blocks performs a similar function with regard to $\ln |F(s)|$.

The Plan Sweep

The plan sweep is used to explore the complex plane in a systematic manner while a pen-dropping comparator indicates points in the plane where $\ln |F(s)|$, $|F(s)|$, or Arg F(s) are equal to some reference value. In this manner, equipotential lines of field problems may be plotted or root loci may be traced.

The jw-sweep unit is employed in its usual capacity except that the axis of scanning is varied in steps across the complex plane to create the path shown in Figure 14.

Automatic realization of this path is accomplished by the circuits represented in Figure 15. A sweep integrator,

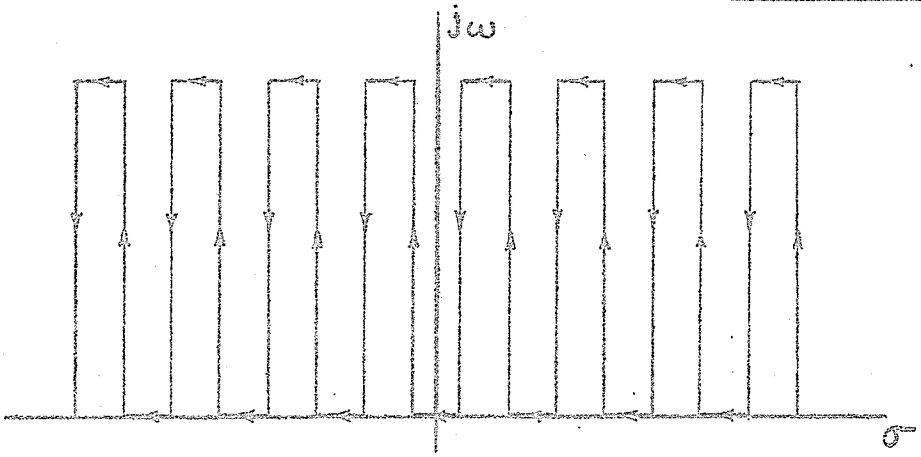

Figure 14. Path of the plan sweep.

with a long time constant, generates a slow ramp of 12.5 minutes duration which is sampled at the end of each jw sweep by a relay gate whose control pulse is derived from potentiometer number two in the jw-sweep unit. Using holding techniques identical to those employed in the jw-sweep unit, a staircase waveform is obtained which is used to modulate a carrier of $6 \angle 0^{\circ}$. The resulting signal is then added to the jw sweep, in the sweep-summation amplifier, to obtain the complete plan sweep. The hold circuit output is also used to drive one axis of the recorder so that the pen position is determined by the value of the variable s.

Often it is desirable to explore only a small portion of the s plane, and the time constant of the integrator may be changed by means of a push-button switch so that s may be

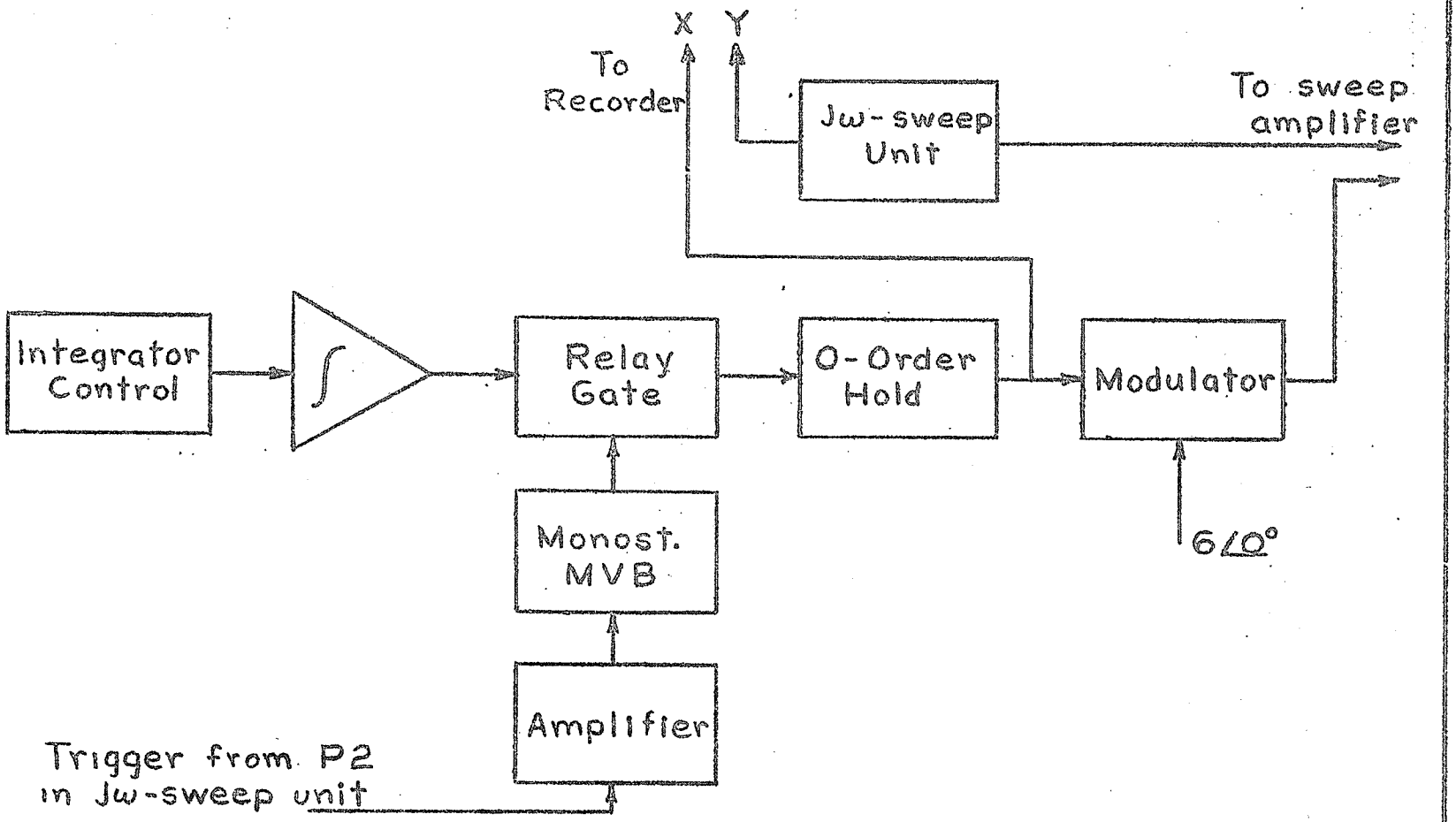

Figure 15. The plan-sweep generator

positioned rapidly before continuing its slow scanning. At the end of a complete scan the integrator is zeroed manually.

III. ANCILLARY UNITS

The Pen-Dropping Comparator

The comparator used in conjunction with the plan sweep is shown in Figure 16. A reference voltage and the computer output are applied to opposite contacts of a chopper modulator whose peak to peak output is equal to the difference between contact voltages. By passing this modulated "difference-carrier" through an amplifier tuned to the carrier frequency, the effect of signal-balanced modulation is obtained. (This, along with other circuit details, is explained in Appendix I.) A peak detector then gives a unipolar output proportional to the difference between the input voltages, regardless of their relative polarities. Further amplification is obtained by two d-c amplifiers. The bias levels of these two amplifiers are so adjusted that when the output of the peak detector falls to zero the pen-dropping circuits are triggered, causing a dot to be made on the paper of the recorder. Since the pen position is determined by the value of s, the location of the dot indicates the value of s at which $|F(s)|$, $\ln|F(s)|$, or Arg F(s), as the case may be, is equal to the reference value.

In order to preserve contact life a variable-reference limiter was placed in front of the chopper so that the

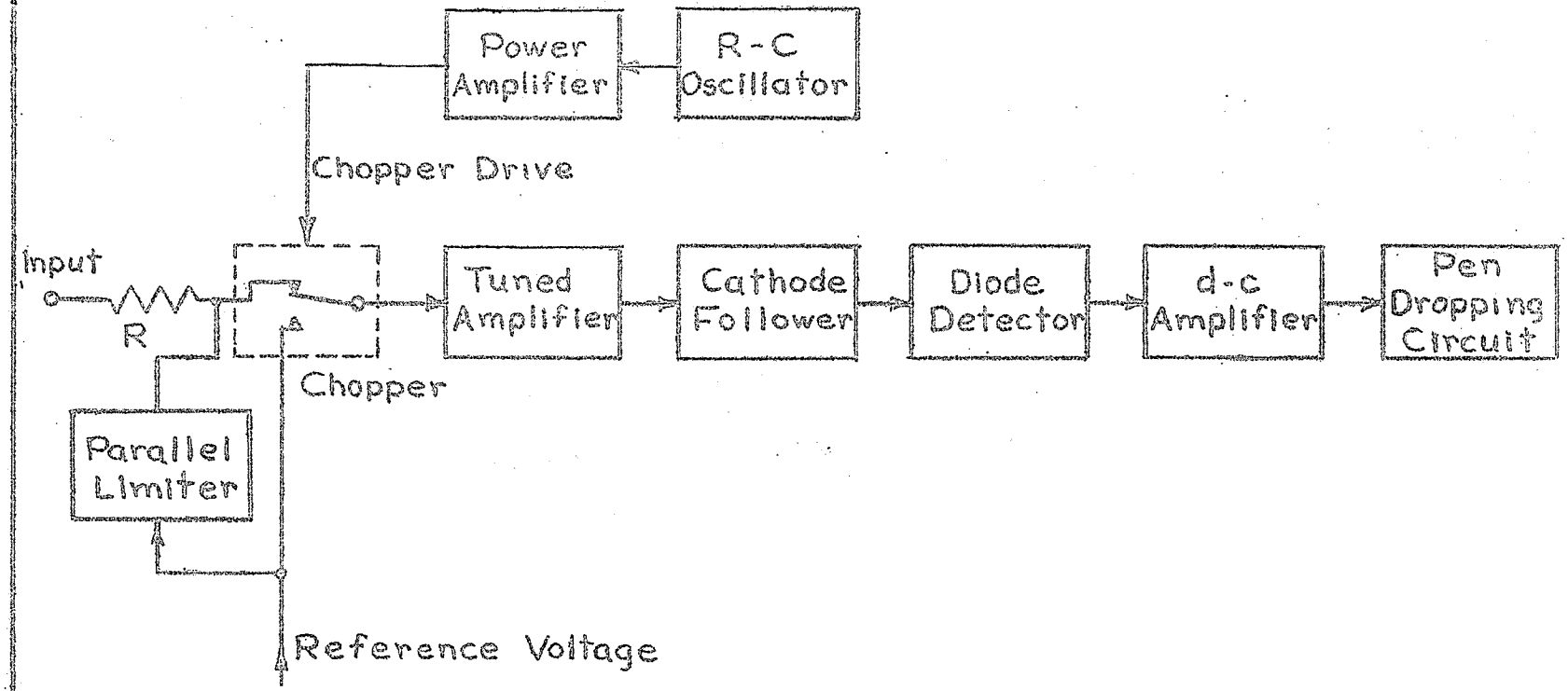

Figure 16. The pen-dropping comparator.

input-contact voltage will never swing more than two volts above or below the reference voltage.

The Error Unit

The error unit (Hi 1) may be used to evaluate differences between two time varying voltages which are analogues of any desired quantities. In the case of the pole-zero machine, one function is generated by the computer, while a second function, for example a desired frequency response curve, is produced by a function generator whose output is a function of w. By means of a level-nulling circuit, any difference in the d-c levels of the two functions may be automatically eliminated so that differences in the relative shapes of the functions become more apparent. Finally, if certain portions of the curves are specially important the error over that portion may be weighted accordingly.

The underlying philosophy, then, is to try to create a function (by positioning poles and zeros) whose characteristics will match those required for a certain job, within reasonable limits. The error unit then becomes a useful tool in the matching process.

A block diagram of the error unit is shown in Figure 17. It may be conveniently divided into three basic sections: (1) error evaluation, (2) level nulling, and (3) mode control. The two modes of operation, namely, error evaluation, and

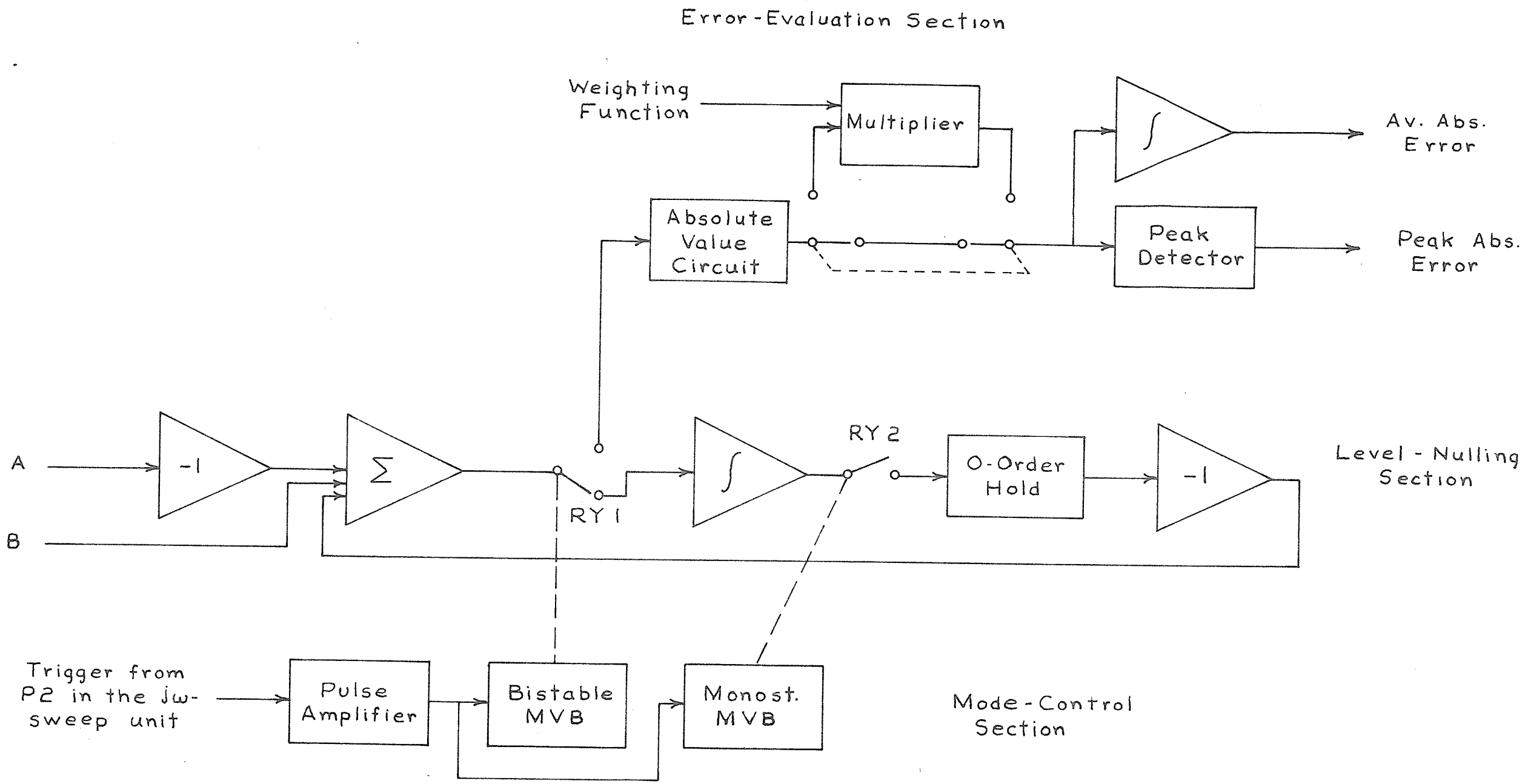

Figure 17. Block diagram of the error unit

level nulling, alternate with each successive jw sweep, and are controlled by binary-driven relays whose control pulses are received via a pulse amplifier from the jw-sweep unit at the beginning of each sweep. These pulses are also utilized by the level-nulling section.

Operation of the remaining sections is as follows: Two time varying functions, A and B, are fed into the unit, where one is inverted and added to the other to obtain their difference. This difference (with RY 1 in the level-null position as shown) is then integrated to give the average error at any time. As the sweep is completed and a new one started, the integrator output is sampled by the momentary closing of RY 2, and held in a zero-order hold circuit. This sampling relay is activated by a monostable multivibrator which receives a trigger at the beginning (end) of each sweep from the pulse amplifier previously mentioned. The hold-circuit output voltage, which remains constant for the duration of the next sweep, is inverted and applied to the difference amplifier at the input so as to eliminate any average differences between the input functions at the difference-amplifier output. In order to function properly, the loop gain of the level-nulling section must be unity, which requires that the sweep period remain constant.

At the same time the integrator output is being sampled, RY 1 is switched to the error evaluation position and the

input to the integrator is removed. The difference, A - B - average difference $\equiv$ e(t), is then applied to the error evaluation circuits as a new sweep begins. The absolute value of e(t) is obtained and applied to an integrator and peak detector whose outputs are the average-absolute error, and peak-absolute error, respectively. If a weighted error is desired the absolute error is routed to an electronic multiplier where it is multiplied by a weighting function before being returned for integration and peak detection. During the next level-nulling sweep the integrator and peak detector are reset to zero in anticipation of a new error-evaluation sweep.

The Antilog Unit

In order to find the magnitude of a function using the pole-zero machine it is necessary to take the antilogarithm of the output. This is accomplished by the antilog unit (Wn 1) shown in Figure 18.

Beginning with the last block, the antilogarithm of E_1 is found by employing an operational amplifier with a logarithmic attenuator in the feedback path. With this arrangement an input swing of .2 volts to 1.78 volts gives an output swing of .1 volts to 100 volts. The chain of amplifiers preceding the antilog amplifier provide for shifting the d-c level of the input as well as changing the gain.

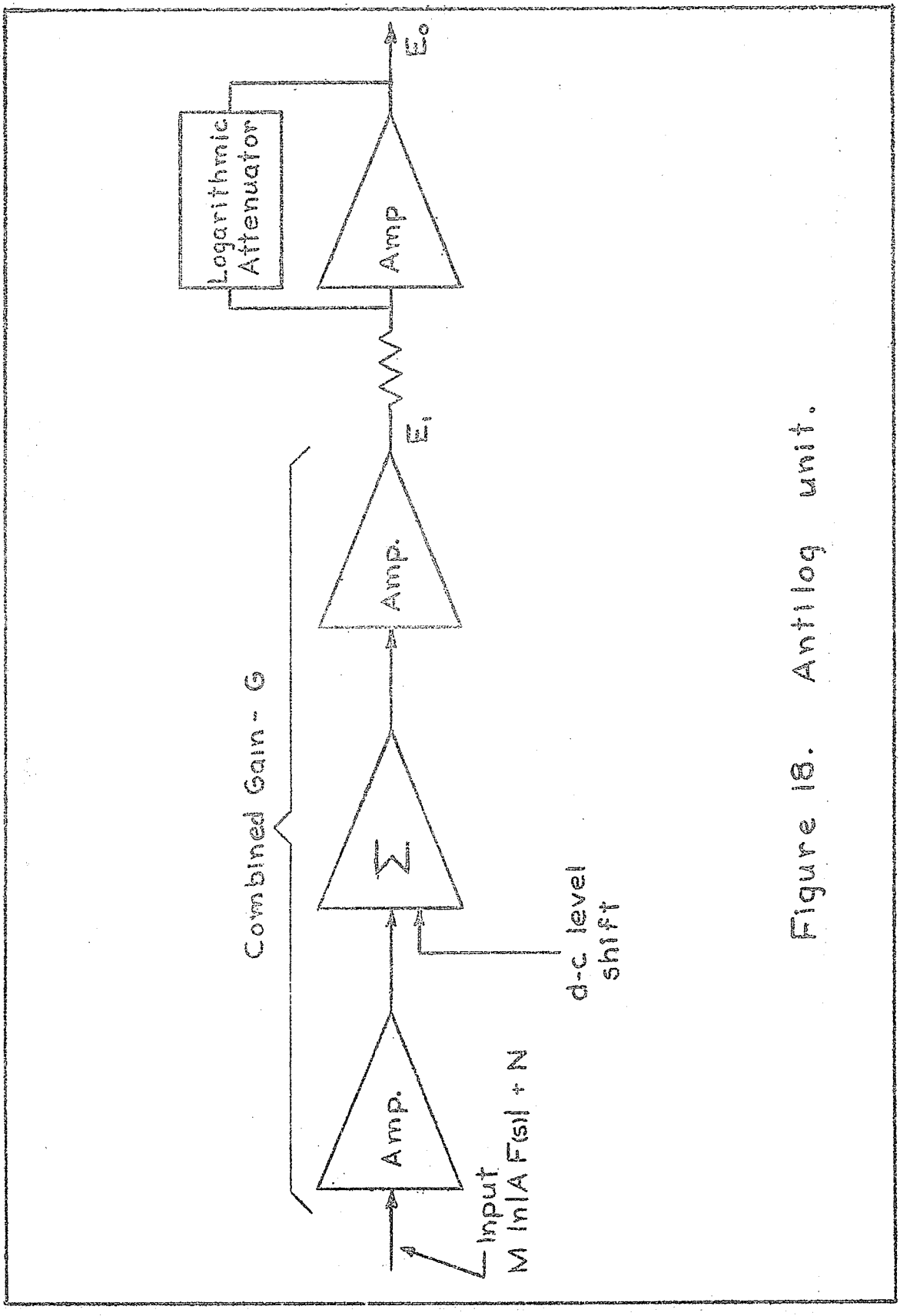

Figure 18. Antilog unit.

The output of the factor-summing amplifier was expressed on page 18 as

$$M \ln|A\ F(s)| + N$$

After passing through the first three stages of the antilog unit, whose overall gain is G, this becomes

$$E_1 = GM \ln|A\ F(s)| + GN + H$$

where H is a d-c level which may be controlled by the input to the second amplifier. Now

$$E_o = \text{Antilog } E_1$$

so that

$$E_o = |A\ F(s)|^{GM}\ e^{GN+H}$$

From this, the term $|F(s)|$ is desired, in which case the product, GM, must be unity and Ae^{GN+H} must be unity. However if F(s) is multiplied by some gain constant there are no serious consequences; in fact it may sometimes be desirable. This gain constant may be controlled by varying H. Thus,

$$E_o = A\ e^{GN+H}\ |F(s)| \qquad (12)$$

CHAPTER III

TESTING OF THE POLE-ZERO MACHINE

In order to evaluate the performance of the pole-zero machine, a variety of tests were carried out covering the various applications of the machine. One test was performed for each typical application. These tests were:

1. A plot of logarithmic magnitude, phase slope and phase versus frequency for a Tchebyscheff Filter.
2. A plot of Nichols Loci for a second order system.
3. A plot of magnitude and phase versus frequency for an impedance function.
4. A plot of equipotential lines about a line charge.
5. A root locus plot.
6. A matching test.

Tests 1 and 2 were designed to determine the accuracy of the logarithmic magnitude, phase slope, and phase sections of the machine, while Test 3 was intended to perform a similar function with respect to the antilog unit. Tests 4 and 5 were carried out to evaluate the performance of the comparator unit and Test 6 provided a means of evaluating the error unit.

I. CALIBRATION

In all cases calibration curves were generated (by the

computer) and recorded along with the test curves to define the horizontal and vertical scales. It was felt that this method was preferable to an absolute calibration which would be susceptible to errors arising from long term drifts. Calibration functions were selected for simplicity, as well as for significant features, such as a peak in the logarithmic magnitude-response curve. For example, the frequency-calibration function almost invariably consisted of a single pole placed near the jw axis at some definite frequency. In this case a peak in the logarithmic magnitude-response curve ($\ln |F(jw)|$), opposite the pole, defined a point of known frequency. Since the frequency scale was known to be linear and the sweep began at zero frequency, the frequency scale was defined.

It may be noted from page 18 that the computer output was of the form

$$M \ln A|F(s)| + N$$

However, this is equivalent to

$$P\ 20 \log_{10} A|F(s)| + N$$

where

$$P = \frac{M}{20 \log_{10} e}$$

Thus, despite the fact that the computer output has been previously discussed in terms of natural logarithms, the output may also be considered in terms of logarithms to the base ten.

Other calibration considerations are less general; they are mentioned in connection with the tests to which they pertain.

II. TESTS

Test 1a: Logarithmic Magnitude Response of a Tchebyscheff Filter

The function chosen for the first test was a Tchebyscheff approximation to the brick-wall function of the ideal low-pass filter. For a fourth order filter with a ripple factor of one, the function is given by

$$F(s) = \frac{.125}{(s+.085+j.946)(s+.085-j.946)(s+.205+j.392)(s+.205-j.392)}$$

A calibration function

$$Fc(s) = \frac{1}{(s+.085+j.946)(s+.085-j.946)}$$

was chosen because its logarithmic magnitude response curve had a sharply defined peak at 0.943 radians and a difference between initial and peak values of fifteen dbv. These two properties allowed the determination of both frequency and logarithmic-magnitude scales.

Both functions were set up on the pole-zero machine and, with the jw sweep in operation, the X-Y recorder was used to plot 20 $\log_{10} |F(jw)|$, and 20 $\log_{10} |Fc(jw)|$ against w.

Although the logarithmic-magnitude scale could be determined from the calibration curve, no absolute logarithmic magnitude values were known since the d-c level of the computer output is arbitrary (it is determined by the number of synthesizers in use and by the bias setting of the factor-summing amplifier). Therefore it was necessary to compute the value of 20 $\log_{10} |F(s)|$ at some convenient but arbitrary point in order to establish a reference. In this particular case the peaks of the Tchebyscheff response were taken as zero dbv.

Test results are shown in Figure 19 along with calculated values (listed in Table I) of 20 $\log_{10} |F(s)|$. It may be seen that the largest error occurred at the highest frequency and was about 1 dbv or 3.7 per cent.

A variety of factors are responsible for the inaccuracy of such a plot, namely:

1. Differences in synthesizer-channel gains.
2. Imperfect logarithmic attenuator characteristics.
3. Inaccurate adjustment of reference phasors.
4. Inaccurate phase lead adjustment of the carrier input to the jw-sweep modulator.

TABLE I

FREQUENCY RESPONSE OF A

TCHEBYSCHEFF LOW-PASS FILTER

$$F(s) = \frac{.125}{(s+.085+j.946)(s+.085-j.946)(s+.205+j.392)(s+.205-j.392)}$$

Frequency radians/sec.	Log Magnitude dbv	Phase Slope deg./rad./sec.	Argument degrees
0.00	- 3.01	142	0
.10	- 2.67	142	- 14
.20	- 1.70	200	- 30
.30	- 0.48	272	- 53
.40	+ 0.02	304	- 83
.50	+ 0.97	252	-112
.60	- 2.33	190	-134
.70	- 3.01	176	-152
.80	- 2.33	232	-171
.90	- 0.23	556	-208
1.00	- 3.01	472	-273
1.10	-10.08	174	-305
1.20	-15.78	98	-318
1.30	-20.32	56	-325
1.40	-24.13	41	-329
1.50	-27.43	40	-333

CALIBRATION FUNCTION

$$Fc(s) = \frac{1}{(s+.085+j.946)(s+.085-j.946)}$$

Frequency radians/sec.	Log Magnitude dbv	Argument degrees
0.0	0.89	0
.94	15.87	- 85
1.0	14.17	-119

Peak Phase Slope - 650 deg./rad./sec.

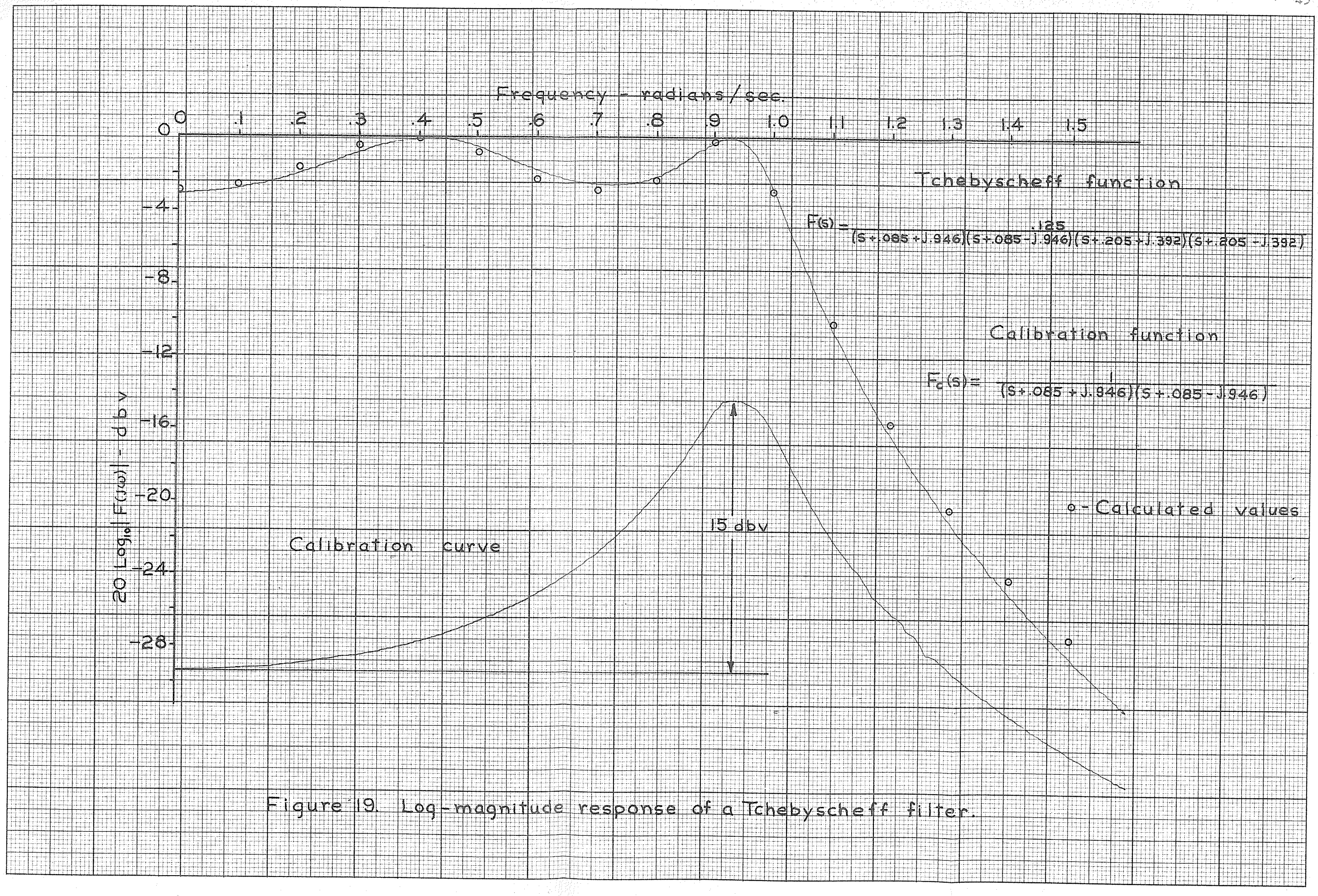

Figure 19. Log-magnitude response of a Tchebyscheff filter.

5. Nonlinearities in the jw-sweep modulator.

Test 1b: Phase and Phase-Slope Characteristics of a Tchebyscheff Filter

Using the same pole configuration as in the previous test, both phase and phase-slope curves were obtained, as shown in Figure 20. The same calibration function was also used, but only phase-slope and phase curves were recorded, the frequency calibration being assumed identical to that of test 1a.

The argument of the calibration function was known to be zero at zero frequency, and its phase at an arbitrarily selected frequency of one radian per second was calculated to be -119 degrees (see Table I). Therefore, the distance corresponding to the phase of the calibration curve at a frequency of one radian per second was used to define the phase scale.

Since the phase of the test function began at zero degrees (the sweep began at zero frequency) no difficulties were encountered concerning an absolute reference.

When compared with calculated values, the largest error in Arg F(s) (as determined by the pole-zero machine) was found to be 14 degrees at a phase lag of 150 degrees, which constituted a maximum error of 9.33 per cent.

In the case of the phase-slope curve, a maximum error of 60 degrees per radian per second, occurring at 330 degrees per

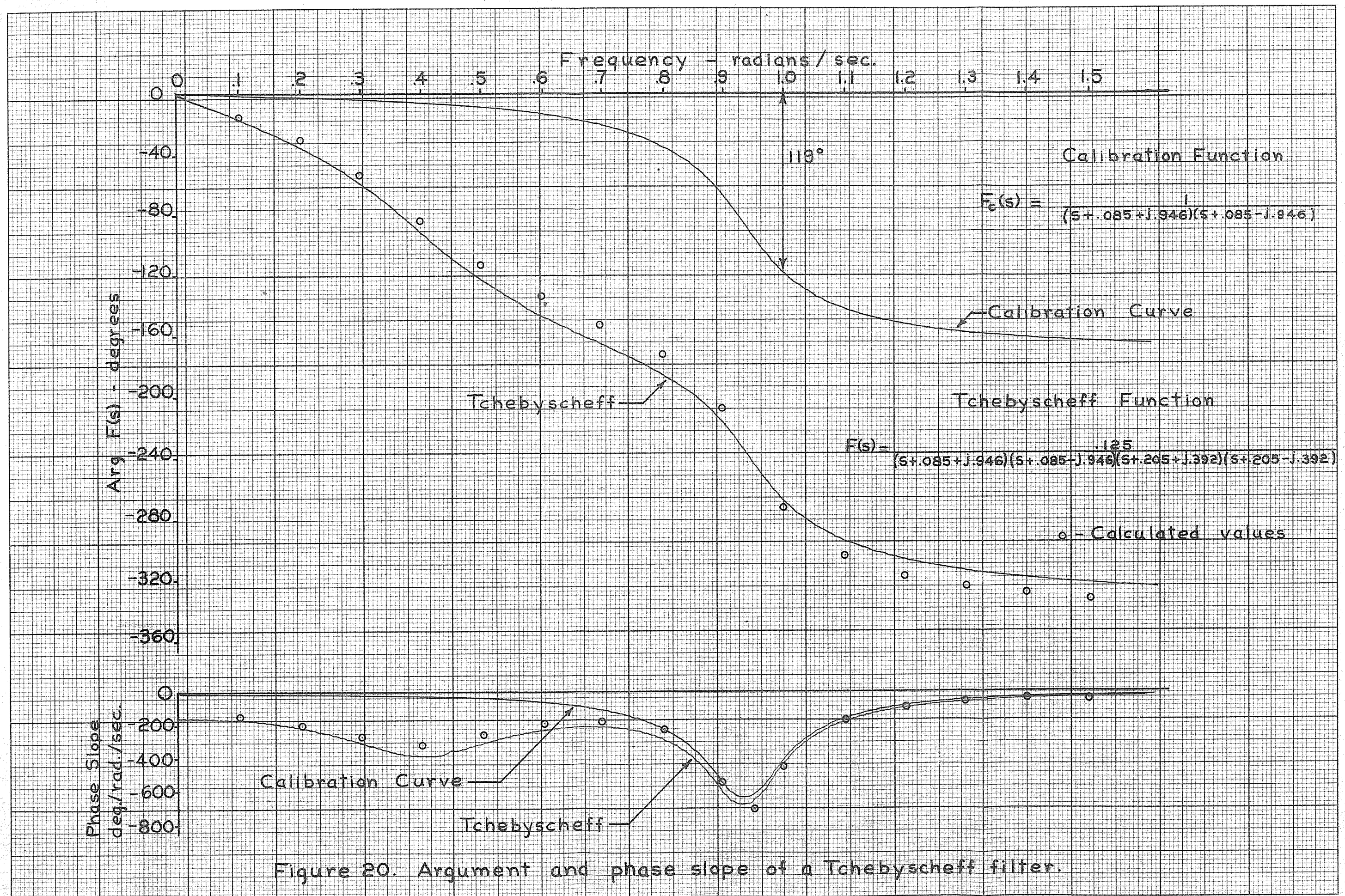

Figure 20. Argument and phase slope of a Tchebyscheff filter.

radian per second, gave a maximum percentage error of 18 per cent.

Since tests of the phase-slope integrator revealed it to be accurate, most of the phase error must be attributed to the inaccuracy of the phase slope determination. Factors which affect this accuracy include those affecting the accuracy of $\ln |F(s)|$, since the phase slope is determined from $\ln |F(s)|$. In addition, the quality of filters used in eliminating the ripple from $\ln |F(s)|$, and the accuracy of the sampling-time adjustment have considerable effect on the accuracy of phase slope as determined by the pole-zero machine. Finally, it must be mentioned that the calibration process, which depends on one point, could introduce significant errors.

Test 1c: Tchebyscheff Response

Both of the preceding tests were carried out several days after the computer had been adjusted; their results are indicative of the average computer performance. However, the same tests carried out immediately after adjustment yielded much more accurate results. The curves, shown in Figure 21, reveal a maximum logarithmic-magnitude error of .33 dbv and a maximum phase error of 10.4 degrees corresponding to a maximum percentage error of 5 per cent. These results were felt to be indicative of the best accuracy attainable, but the rapid

Tchebyscheff function

$$F(s) = \frac{.125}{(s+.085+j.946)(s+.085-j.946)(s+.205+j.392)(s+.205-j.392)}$$

Log-mag. calibration function

$$F_M(s) = \frac{1}{(s+.085+j.946)(s+.085-j.946)}$$

Phase calibration function

$$F_p(s) = \frac{1}{(s+.15+j.5)(s+.15-j.5)}$$

Phase response

Phase

Calibration curves

Log Mag.

Log-Magnitude response

20 Log$_{10}$ |F(jω)| - dbv

Arg F(jω) - degrees

0 -4 -8 -12 -16 -20 -24 -28

0 -40 -80 -120 -160 -200 -240 -280 -320 -360

0 .1 .2 .3 .4 .5 .6 .7 .8 .9 1.0 1.1 1.2 1.3 1.4 1.5

Frequency - radians / sec.

Figure 21. Tchebyscheff response.

deterioration in accuracy after several days denotes relatively serious drift problems.

Test 2: Nichols-Loci Plots

The pole-zero machine was connected to the X-Y recorder in such a way that logarithmic magnitude was plotted against phase as s varied along the jw axis. For test purposes, the transfer function of a second-order system was chosen, which was of the form

$$F(s) = \frac{1}{(s^2 + 2\zeta s + 1)}$$

A value of $\zeta = 1$ was selected for the test function while $\zeta = .05$ was adopted for a calibration function. The resulting calibration curve had a well-defined peak in the Nichols Plane suitable for magnitude calibration. In addition, the curve rapidly approached a 180 degree asymptote which enabled a phase calibration.

The test results are shown in Figure 22. In this case errors cannot be specified as being entirely due to magnitude or phase because they are interdependent. Nevertheless, maximum deviations from the correct values were 3 dbv in logarithmic magnitude and 8 degrees in phase. (Actual values of the Nichols loci are listed in Table II. They were taken from Gille, Pelegrin, and Decaulne [Gi 1]).

TABLE II

MAGNITUDE AND PHASE OF

$$F(s) = \frac{1}{(s^2 + 2\zeta s + 1)}$$

Test Function $\zeta = 1$

Phase degrees	Logarithmic Magnitude dbv
0	0.0
- 30	- .8
- 60	- 2.7
- 90	- 5.3
- 120	-12.3
- 150	-24.1

Calibration Function $\zeta = .05$

Phase degrees	Logarithmic Magnitude dbv
0	0.0
- 30	19.6
- 60	19.0
- 90	20.0
- 120	18.4
- 150	12.8

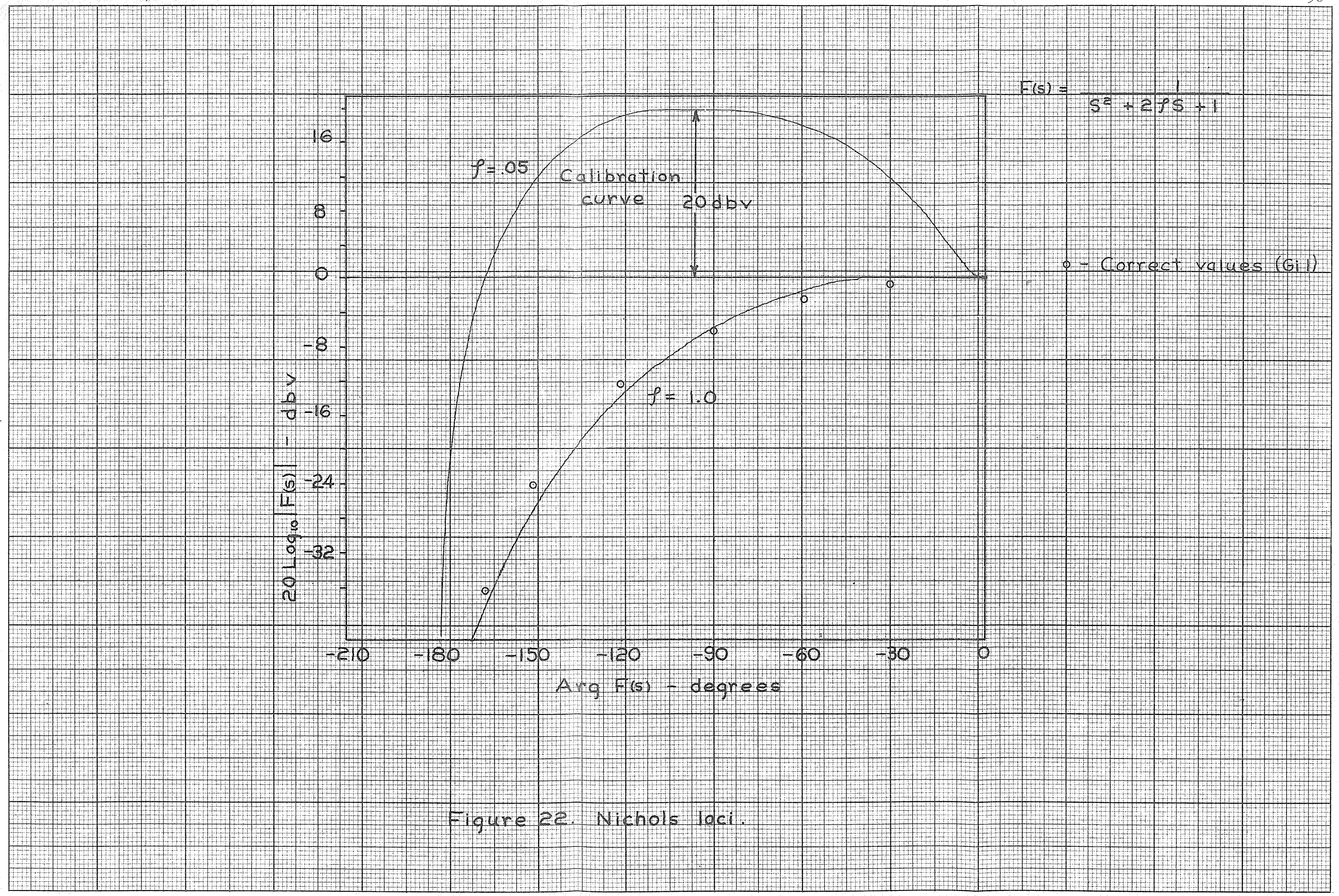

Figure 22. Nichols loci.

It is also possible to define a vector error, similar to the "vector margin" defined by Smith (Sm 1) for specification of stability in the L plane. However, to measure this error directly from the Nichols loci requires that one radian on the phase scale correspond to one neper on the magnitude scale, the vector being measured in complex nepers. Since the scales of Figure 22 do not comply with the above requirement it was only possible to estimate the point at which the maximum vector error occurred. For the point chosen, the vector error was .12 + j.06 nepers.

Test 3a: Magnitude of an Impedance Function

The impedance function utilized in this test was one used by Bridges (Br 1) in tests on a potential analogue of the complex plane. It is given by:

$$Z(s) = \frac{(s + 20)(s + 10 + j40)(s + 10 - j40)}{(s + 10 + j20)(s + 10 - j20)}$$

In this test the antilog unit was employed to calculate $|Z(s)|$ from $\ln|Z(s)|$. However, its use introduced certain complications in the selection of a calibration function. As was indicated in the section on the antilog unit (page 37), the output of the antilog unit is $Ae^{GN+H}|F(s)|$ where N is the d-c level of the factor-summing amplifier due to the d-c levels of synthesizer channels. This d-c level, which controls

the gain constant, Ae^{GN+H}, depends on the number of channels switched on, and is different for each channel, so that, in order to have the same gain constant for both test and calibration functions, the calibration function must use the same channels and therefore the same number of poles and zeros as the test function. In the above case, it was possible to comply with the restriction on the number of poles and zeros while still retaining a simple function by using two poles to cancel two zeros. Thus the calibration function used was

$$Fc(s) = (s + 20)$$

For calibration purposes the magnitudes of the test and calibration functions were calculated, at $s = j0$, to be 68 ohms and 20 ohms respectively. Then, the distance between the starting points of the two curves was taken to be 48 ohms, which defined the magnitude scale.

The test results are shown in Figure 23 along with the calculated values from Table III. A maximum deviation of 7 ohms in 94 ohms constituted a maximum error of 7.5 per cent. Although this is not a true indication of antilog unit accuracy, because the logarithmic magnitude input was not necessarily correct, the results indicate the overall accuracy obtainable. (Tests on the antilog unit by Woon-Sam [Wn 1] indicated a linearity of 2 per cent when the logarithm of the output was plotted against the input.)

TABLE III

COMPUTED IMPEDANCE MAGNITUDE AND PHASE OF

$$Z(s) = \frac{(s + 20)(s + 10 + j40)(s + 10 - j40)}{(s + 10 + j20)(s + 10 - j20)}$$

Frequency radians/sec.	Magnitude ohms	Phase degrees
0	68.00	0.0
4	70.09	4.64
8	76.24	7.23
12	85.53	5.72
16	94.14	- 1.54
20	93.30	-13.88
24	78.57	-25.68
28	58.84	-30.98
32	42.47	-27.87
36	31.68	-16.22
40	26.51	2.34
44	26.15	22.08
48	28.86	37.57
52	33.05	48.25
56	37.81	55.43
60	42.76	60.48
64	47.72	64.10
68	52.64	66.91
72	57.49	69.09
76	67.26	70.86

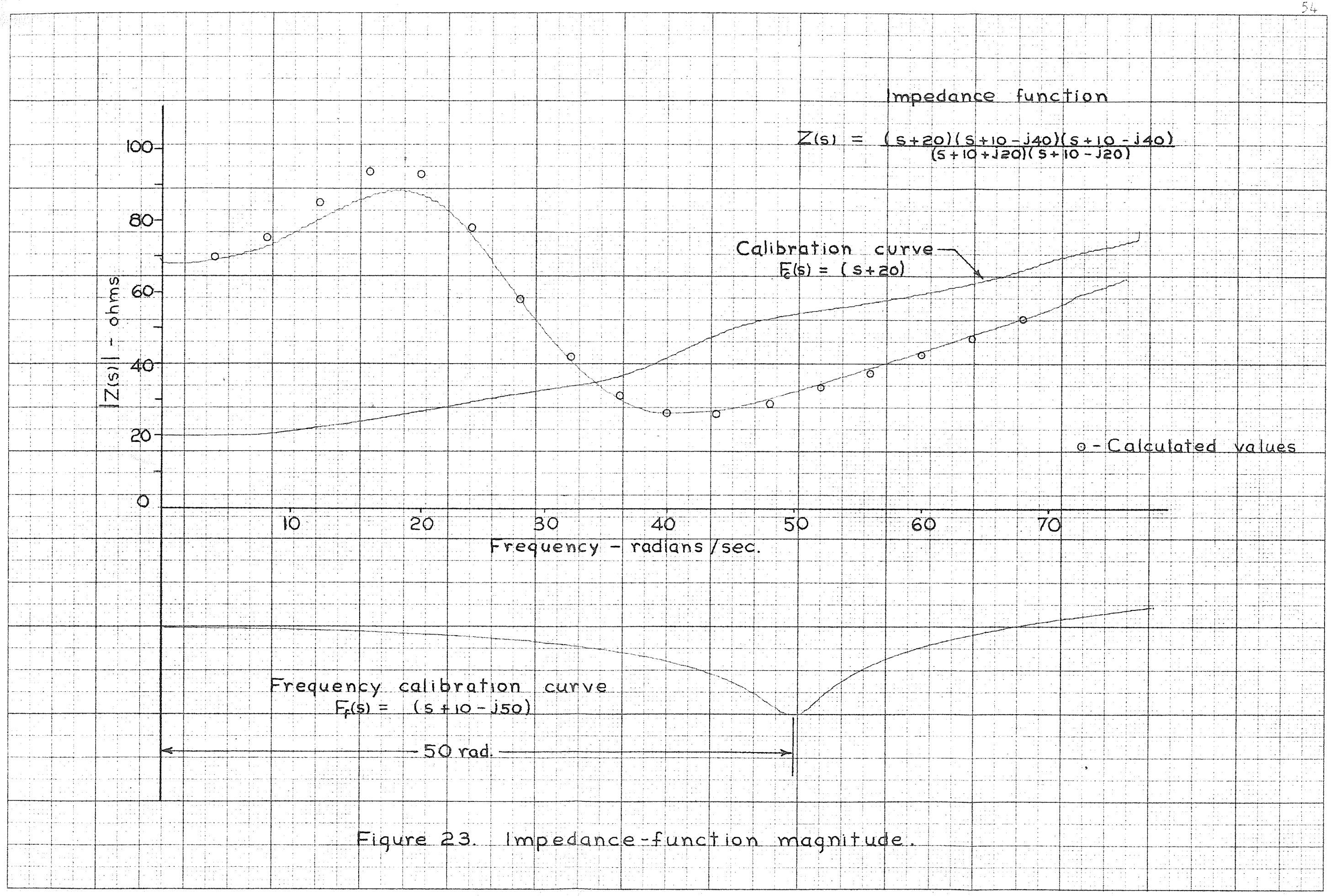

Figure 23. Impedance-function magnitude.

Test 3b: Phase Characteristic of an Impedance Function

As a further check of phase accuracy, the argument of Z(s) versus w was plotted in Figure 24 along with the phase-slope curve, although the latter was included only to show its general shape. A calibration function of

$$Fc(s) = s + 10$$

gave a phase shift of 45 degrees at s = j10 and had an argument of 0 degrees at s = j0 which served to define the phase scale. The maximum error was about 3 degrees and although this was 25 per cent of the total phase at that point, the results may be considered as reasonably good. In fact any phase characteristic which oscillates about the zero degree phase point may be expected to have high percentage errors. This is due to the method of determining phase by integration of phase-slope, a method which tends to accumulate errors.

Test 4: Equipotential Lines About a Line Charge

The potential at a point due to several line charges (see Figure 26)

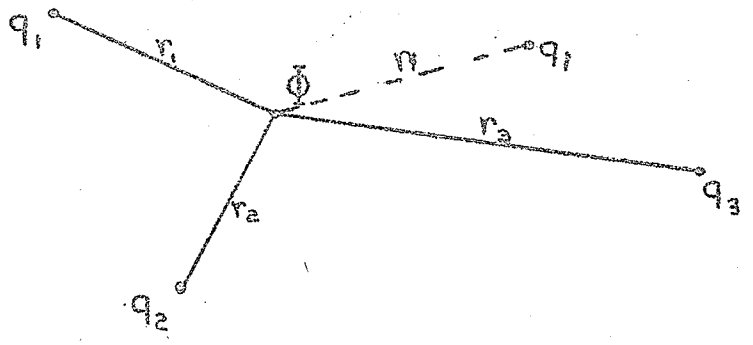

Figure 26. Line charges.

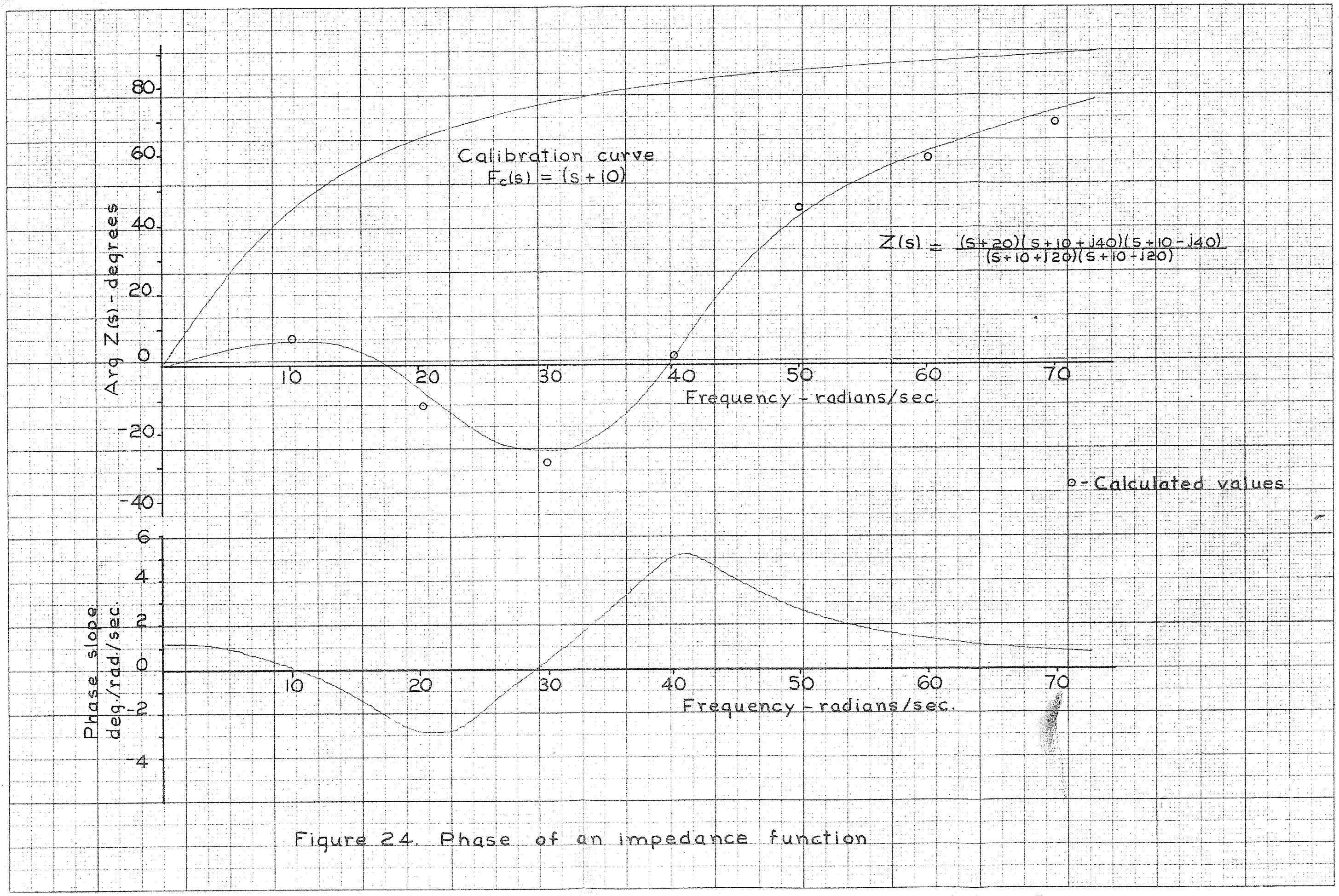

Figure 24. Phase of an impedance function

is given by

$$\phi = - \sum_{i=1}^{n} \frac{q_i}{2\pi\epsilon} \ln r_i$$

where r_i is the perpendicular distance from the line to the point where the potential is being determined, and q_i is the charge per unit length carried by the line. This is the type of calculation performed by the pole-zero analogue computer, and by utilizing the pen-dropping comparator it was found that equipotential lines could be plotted. Since it was desired to check the accuracy attainable, only the equipotential lines about a single line charge were plotted, so that any deviation from a perfect circle would indicate the inaccuracies of the computer.

In order to calibrate the plane the following procedure was followed. First the pen driving voltages from the plan sweep (jw and σ) were connected to the X-Y recorder and the axes of the plane were defined by noting the pen position at which the s phasors became zero. A pole was then placed at $s = 10 + j0$ and a magnitude response curve was plotted ($\ln |F(s)|$ against σ), while w remained at zero. This curve had a peak at $\sigma = 10$, so the X-Y recorder gain, in the σ direction, was adjusted so that the peak occurred at a convenient distance from the origin, the exact distance being noted. Then a pole was placed at $s = 0 + j10$ and the above

procedure was repeated, plotting ln $|F(s)|$ against w. The X-Y recorder gain in the w direction was then adjusted so that ten units in the w direction corresponded to the same distance as ten units in the σ direction.

Upon completion of the calibration, a pole was placed at $s = j10$ and the computer output, ln $|F(s)|$, was connected to the comparator. An arbitrary reference voltage of -5 volts was set and the plan sweep started. The results of the first scan are shown in Figure 27 as the innermost ring of crosses. Three additional sweeps were made with the comparator reference at 0, 5, and 10 volts, yielding the other three rings. As Figure 27 shows, the rings produced were not perfectly circular, with the largest deviation being .24 units. A deviation of .18 units in 3 gave a maximum percentage deviation of 6 per cent. Such inaccuracies are due to the comparator, and inaccuracies in the computation of ln $|F(s)|$ by the pole-zero machine.

It must be mentioned that the "x" marks are not the points actually plotted by the comparator but are points located midway between consecutive points plotted by the comparator. The reason for this is as follows. The chopper available for use in the comparator was relatively noisy, having a peak to peak output of 25 millivolts with the input grounded. Also, the pen-dropping circuit is triggered by a

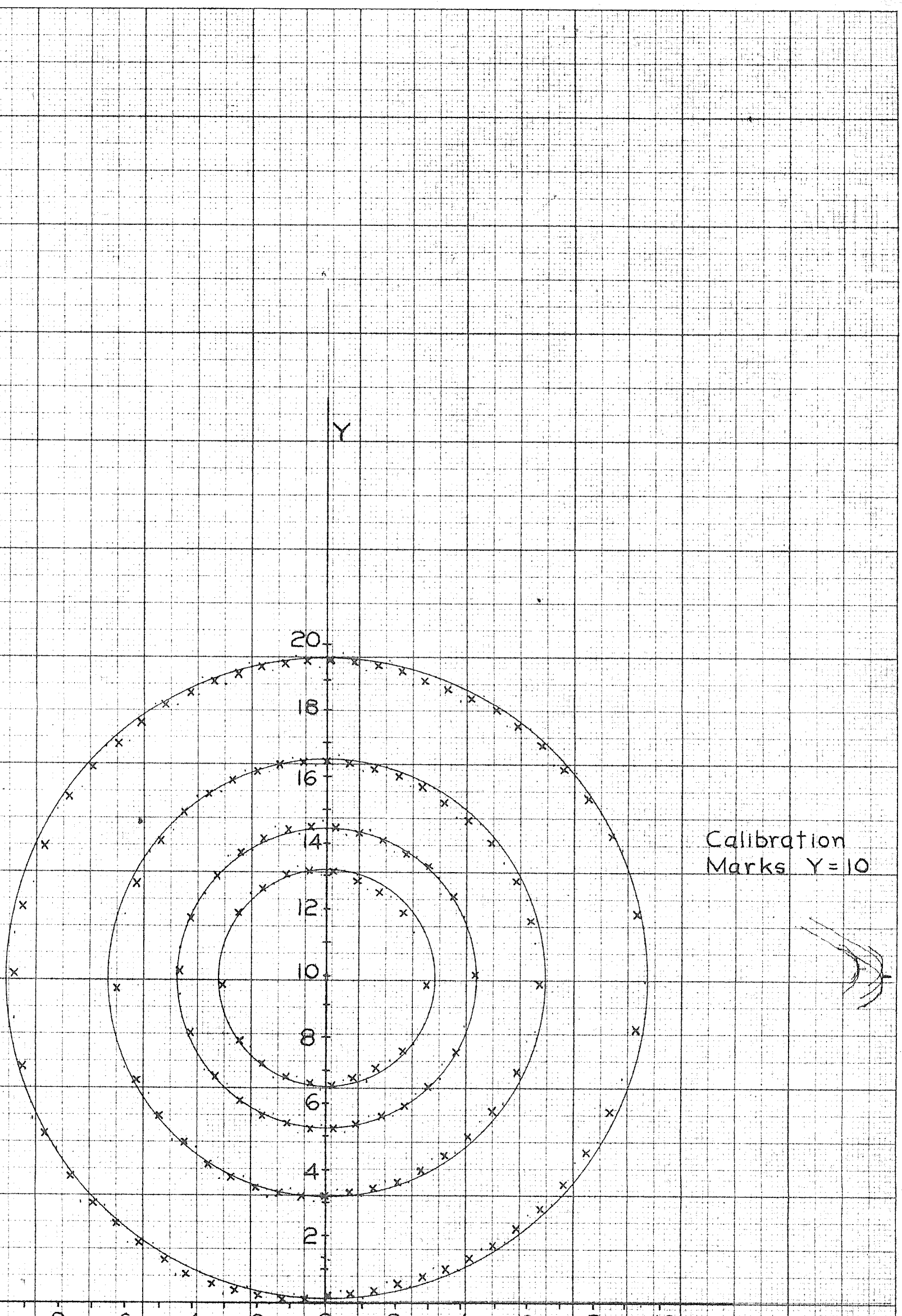

Figure 27. Equipotential lines about a line charge

waveform of the type shown in Figure 28b (as explained in Appendix I) whenever the input voltage reaches the reference level. The effect of the chopper noise is to reduce the sharpness of the peak so that the circuit must be adjusted to drop the pen slightly before the reference value is reached, as indicated in Figure 28c.

The results of this "lead effect" are illustrated in Figure 29 for an equipotential line. Dot, d_1, is

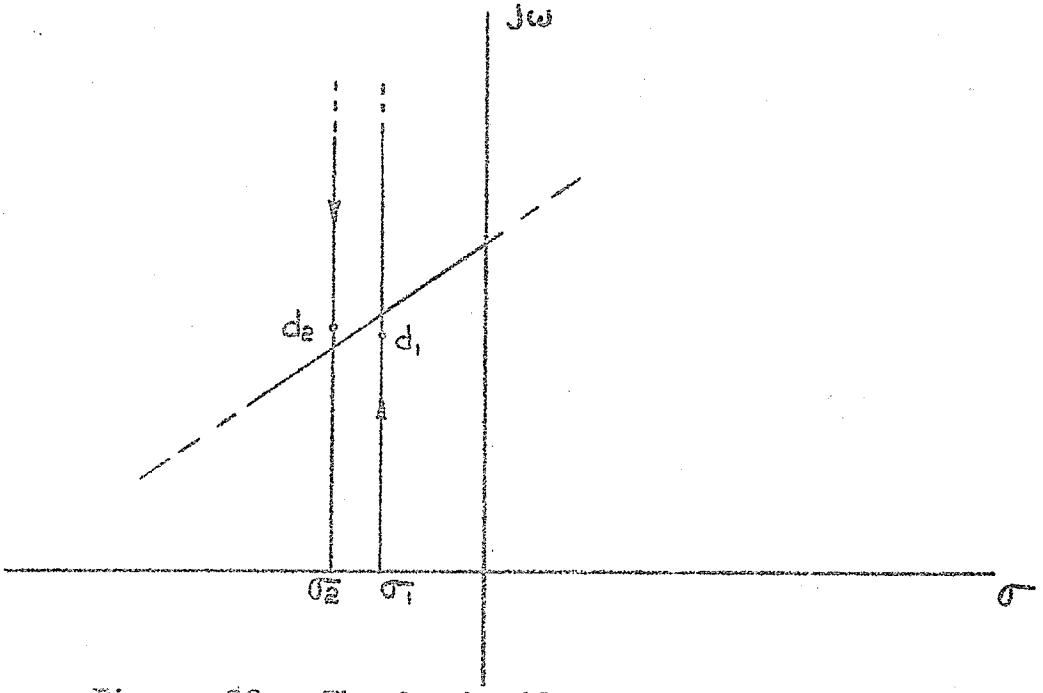

Figure 29. The lead effect.

plotted as the variable s approaches the line from one side and dot, d_2, is plotted as s approaches from the other, as shown. If the equipotential line is assumed to be straight

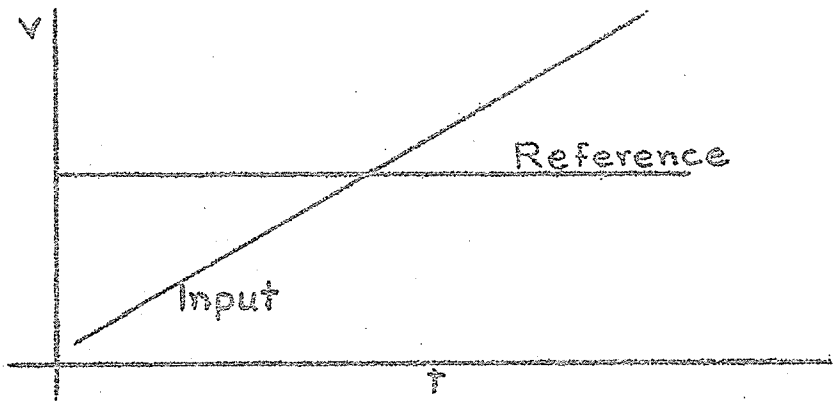

a. Chopper Input

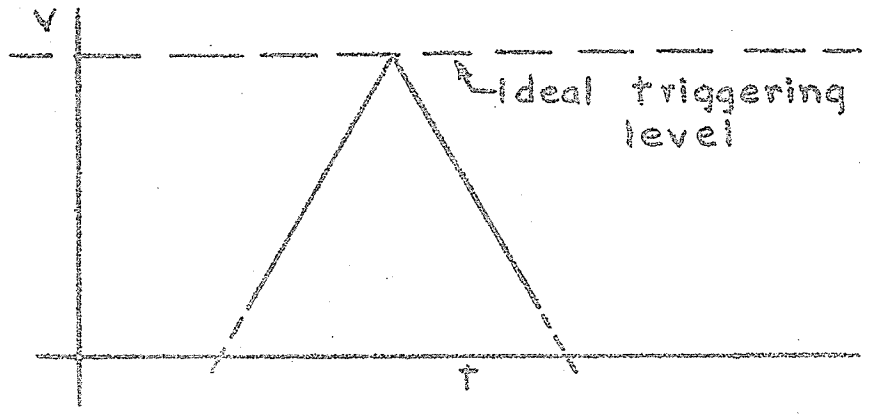

b. Trigger to pen-dropping circuit

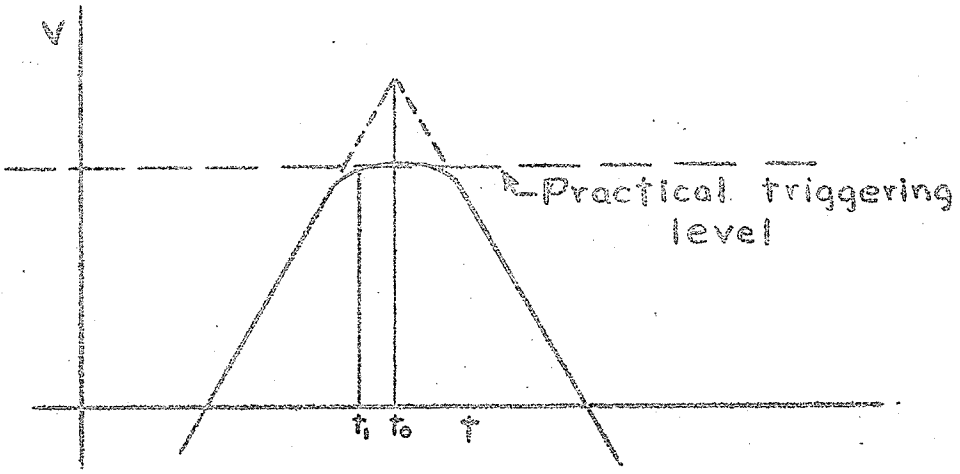

c. Effect of chopper noise

Figure 28. Comparator waveforms.

in the region between σ_1 and σ_2, then a point on the equipotential line is defined by the midpoint of a straight line joining d_1 and d_2. This requires the additional assumption that the same amount of lead is present in each case. Both assumptions are reasonable considering the small difference between σ_1 and σ_2 for the plan sweep.

In its present form the pole-zero machine is not capable of solving general problems with non-integer values of line charge since the gain of each factor-synthesizer channel is the same. By making the gain of each channel variable it would be possible to simulate line charges of any relative magnitudes. Nevertheless, the foregoing test serves to illustrate the machine's application in this field.

Test 5: A Root-Locus Plot

Root-locus plots are employed in the design of feedback-control systems to provide a clear picture of closed loop response. If such a system has the transfer function

$$\frac{K\,F(s)}{1 + K\,F(s)}$$

the root locus is defined (Bw 1) as the locus of points where

$$K\,F(s) = -1$$

as K ranges from zero to infinity. This is simply the locus of points at which

$$\text{Arg } F(s) = n\pi \text{ , } n \text{ odd}$$

and may be plotted by use of the pen-dropping comparator in conjunction with the plan sweep.

For the test, F(s) was chosen to be:

$$F(s) = \frac{1}{(s + 5)(s + 10 - j8)(s + 10 + j8)}$$

The complex plane (as seen on the X-Y recorder) was calibrated in the same manner as in Test 4. In addition, it was necessary to set the comparator-reference voltage to correspond to an argument of 180 degrees. This was accomplished by placing a function with accurately known phase characteristics on the computer and then, with the jw sweep in operation, adjusting the comparator-reference voltage so that the pen dropped as the 180 degree point was crossed.

After calibration, the test function was fed into the machine and the root locus plotted. This locus is shown in Figure 30 along with the correct locus, calculated by a digital computer. (The calculated values are given in Table IV for various values of K.)

Figure 30 shows large inaccuracies which are primarily due to the inaccurate determination of argument by the

TABLE IV

ROOT LOCUS OF

$$K\,F(s) = \frac{K}{(s + 5)(s + 10 - j8)(s + 10 + j8)}$$

K	Real Root	Complex Conjugate Roots	
		real part	imaginary part
0	- 5.00	-10.00	±8.00
100	- 6.28	- 9.36	7.67
200	- 7.93	- 8.54	7.46
300	- 9.68	- 7.66	7.55
500	-12.24	- 6.37	8.19
700	-13.86	- 5.56	8.86
900	-15.05	- 4.97	9.46
1100	-16.00	- 4.50	9.98
1500	-17.49	- 3.75	10.88
1900	-18.66	- 3.16	11.64
2500	-20.08	- 2.45	12.62
3100	-21.25	- 1.87	13.45
4100	-22.86	- 1.06	14.63
5100	-24.20	- .40	15.63
7000	-26.27	.63	17.23
9300	-28.62	1.80	19.08
11700	-30.07	2.53	20.24
14200	-31.65	3.32	21.52
19200	-34.31	4.60	23.70

$$F(s) = \frac{1}{(s+5)(s+10-j8)(s+10+j8)}$$

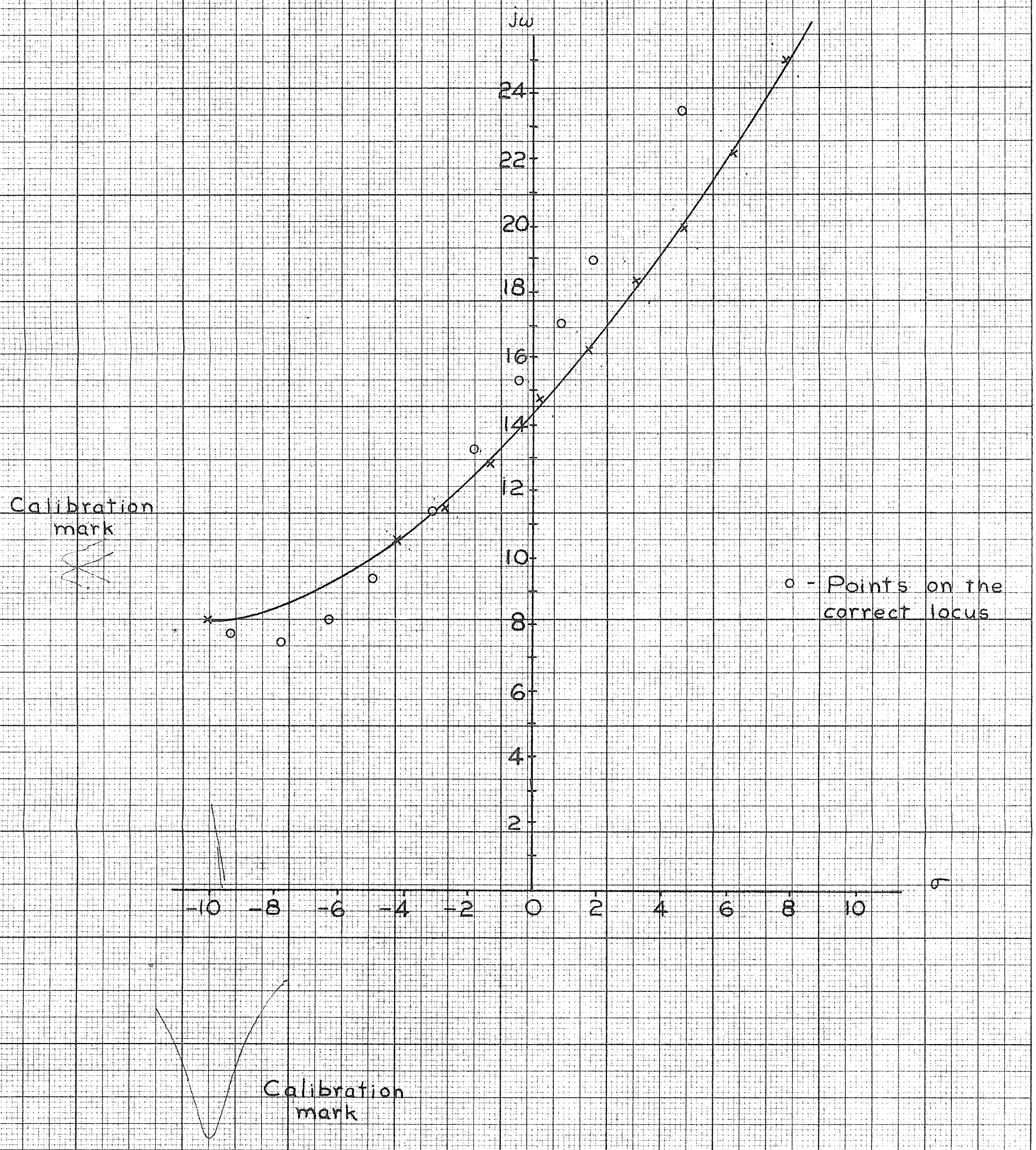

Figure 30. Root-locus plot.

pole-zero machine. Even though errors in phase may be small, they can give rise to large errors in the position of the root locus in regions where the phase slope is small. Consequently, the pole-zero machine seems unsuitable for plotting accurate root loci without a drastic improvement in the accuracy of phase determination.

Test 6: Function Matching

One of the more important applications of the pole-zero analogue computer lies in rational approximation of magnitude or phase-response characteristics by positioning poles and zeros. Once the pole and zero positions are known it is possible to construct a network with the required features using methods of network synthesis. In this discourse, only the problem of finding the appropriate pole-zero configuration is discussed.

Of two possible approaches to matching functions, the simplest involves drawing the desired function on the X-Y recorder to the same scale as the computer output (which may be determined from a calibration curve). The computer output is then observed while pole and zero positions are varied to obtain a satisfactory approximation to the desired response.

To provide a check on the sensitivity of this method, a function was drawn on the X-Y recorder by the computer, after which the pole positions were altered. An inexperienced

operator was then asked to vary the pole positions so as to obtain a computer output resembling, as closely as possible, the original curve. Ideally, the computer output would coincide with the original curve if the poles were returned to their initial positions.

The function chosen was the Tchebyscheff function of Test 1, with poles located at

$$s = .085 \pm j.946$$
$$s = .205 \pm j.392$$

After the magnitude response curve had been run, the poles were relocated at

$$s = .3 \pm j.6$$
$$s = .5 \pm j.1$$

An operator then adjusted the pole positions to give the best fit. The results for three different operators are shown below:

1. Operator 1 relocated poles at

$$s = .080 \pm j.930$$
$$s = .190 \pm j.390$$

Maximum error was 7.5 per cent.

2. Operator 2 relocated poles at

$$s = .085 \pm j.950$$

$$s = .205 \pm j.40$$

Maximum error was 2 per cent

3. Operator 3 relocated poles at

$$.085 \pm j.985$$

$$.200 \pm j.390$$

Maximum error was 4 per cent

The foregoing results, which were obtained in the average time of fifteen minutes, indicate that the method is practical. The solution time could be reduced considerably by an experienced operator, although a limit is set by the sweep period of fifteen seconds. A faster sweep could be employed if a CRO were used for display purposes but only preliminary adjustments would be possible, and the X-Y recorder would have to be used for final adjustments.

The second matching technique involves the use of the error sensing unit. Unfortunately, the lack of sensitivity of the present unit prevented any conclusive tests. However, the unit should prove valuable when dealing with functions in which some regions must be matched very closely while others are less important. (That is, when weighted errors must be considered.) In addition, the error unit may be used to

advantage in conjunction with the first method by making the average error available. It could be even more useful if a switch were provided to allow starting and stopping of the integration at any time so that average errors over small regions could be measured.

CHAPTER IV

CONCLUSIONS

It must be stated at the outset that the foregoing tests do not represent an exhaustive investigation of the pole-zero analogue computer. However, they do indicate the possibilities of the computer and serve to illustrate its manifold applications.

I. EVALUATION

A critical evaluation of the machine may be made by contrasting it with other analogue computers of a similar nature on a point by point basis.

Logarithmic-Magnitude Calculation

The accuracy of logarithmic-magnitude calculations by the pole-zero machine is comparable to that of the Complex-Plane Scanner at Columbia University (Kr 1; Al 1), which is not surprising since the two computers are nearly identical in terms of circuitry used for logarithmic-magnitude calculations.

In comparison with the potential analogue, the pole-zero machine is less accurate over limited frequency ranges, but it is not subject to the "infinity-circle" errors (Br 1) of the potential analogue.

The accuracy of the machine depends primarily on the quality of the logarithmic attenuators (which could be improved).

Phase Calculation

The pole-zero machine is capable of producing slightly more accurate phase calculations than those obtained from a potential analogue at the University of Manitoba. Conversely, the pole-zero machine is much less accurate with regard to phase determination than the Complex-Plane Scanner (Kr 1; Al 1), which accurately measures phase to within 1 degree. This accuracy is possible because phasemeters are employed to measure phase, and although they require a large number of components, the saving in circuitry by use of the horizontal-sweep method is offset by the increase in complexity and the critical nature of the circuitry required. In particular, electronic modulators are required which must be compensated for undesirable phase shifts, and filters employed to remove the ripple from $\ln |F(s)|$ must be, as nearly as possible, ideal. It is felt that these filters are the primary source of error in phase determination and could be improved significantly.

Ancillary Units

The ancillary units have no counterparts in other similar analogue computers, but they constitute a definite

step forward in increasing the versatility of the computer. Undoubtedly, there is room for improvement, notably, in an increase in the sensitivity of the error unit and the use of a better chopper in the pen-dropping comparator.

II. APPLICATIONS

In the field of analysis, a well-programmed digital computer can give results superior to those of the pole-zero machine, although the latter has some advantages in ease of setting up the problem and speed of computation. Also, many engineering applications do not require the high accuracy obtainable with a digital computer. However, the chief application of the pole-zero machine lies in the field of approximating response functions by experimentally positioning poles and zeros. Its ability to do this could be greatly enhanced by improving the stability of the machine to the point where an absolute calibration was possible. This would eliminate the need for running calibration curves each time the machine was used.

BIBLIOGRAPHY

Al 1 Alaia, C. M., and Oden, P. H., "Complex-Plane Scanner - Final Report," Technical Report T-26/B, Columbia University, New York, 27, N.Y.; Jan., 1958.

Bo 1 Boothroyd, A. R., Cherry, E. C., and Makar, T., "An Electrolytic Tank for the Measurement of Steady-State Response, Transient Response and Allied Properties of Networks," Proc. IEE, vol. 96, part I, pp. 163-177; May, 1949.

Bi 1 Bigelow, S., and Wuorinen, J., "Extended Angular Range Direct-Reading Phasemeter," Rev. Sci. Inst., vol. 28, pp. 713-717; Sept., 1957.

Br 1 Bridges, E., "A Network-Function Simulator," M. Sc. Thesis, University of Manitoba; 1958.

Bw 1 Bower, J. L., Schultheiss, P. M., Introduction to the Design of Servomechanisms, John Wiley and Sons, Inc., New York, 1958, Chapter 9.

Gi 1 Gille, J-C, Pelegrin, M. J., Decaulne, P., Feedback Control Systems, McGraw-Hill Book Company, Inc., New York, 1959, p. 94.

Ha 1 Harries, J. H. O., "The Rubber Membrane and Resistance Paper Analogies," Proc. IRE, vol. 44, pp. 236-248; Feb., 1956.

Hi 1 Hill, J. D., "An Error Sensing Unit for the Complex-Plane Scanner," M. Sc. Thesis, University of Manitoba; 1960.

Kr 1 Kranc, G., Mauzey, P., and Wuorinen, J., "Complex-Plane Scanner - An Analogue Computer," Technical Report T-2/F, Columbia University, New York, 27, N.Y.; Aug., 1955.

Ra 1 Ragazzini, J. R., and Reynolds, G., "The Electronic Complex-Plane Scanner," Rev. Sci. Inst., vol. 24, p. 523; July, 1953.

Se 1 Seshu, S., and Balabanian, N., Linear Network Analysis, John Wiley and Sons, Inc., New York, 1959, pp. 276-286.

Sm 1 Smith, O. J. M., Feedback Control Systems, McGraw-Hill Book Company, Inc., New York, 1958, p. 9.

Va 1 Valstyn, E. P., "A Complex-Plane Scanner," M. Sc. Thesis, University of Manitoba; 1958.

Wa 1 Wagerer, H. F. J., "A System for the Computation of the Phase of Network Functions by the Complex-Plane Scanner," M. Sc. Thesis, University of Manitoba; 1959.

Wn 1 Woon-Sam, J. L., "Logarithmic and Antilogarithmic Amplifier Circuits," M. Sc. Thesis, University of Manitoba; 1959.

APPENDICES

APPENDIX I

THE PEN-DROPPING COMPARATOR

Since the operating principle and some of the circuits of the comparator are unconventional, it was felt that a more detailed account of its operation was warranted. It is assumed at this point that the general account of the comparator has been read. (Chapter II).

I. OPERATING PRINCIPLE

Although the following scheme may have been employed elsewhere, its application is unknown to the writer. Consequently, the theory is presented in detail.

Consider a single-pole, double-throw chopper, with a d-c reference voltage applied to one contact and a slowly varying signal applied to the other. (By "slowly varying" is meant a waveform in whose frequency spectrum the highest significant frequency component is much less than the chopping frequency.) Let the input waveform be $V(t)$, the chopping frequency be w_o and the reference voltage be V_r. For the input, $V(t)$, shown in Figure 31, the chopper output, V_c, will be as shown in Figure 32.

The equation of the function shown in Figure 32 may be found by noting that Vc is the result of multiplying $(V(t) - V_r)$

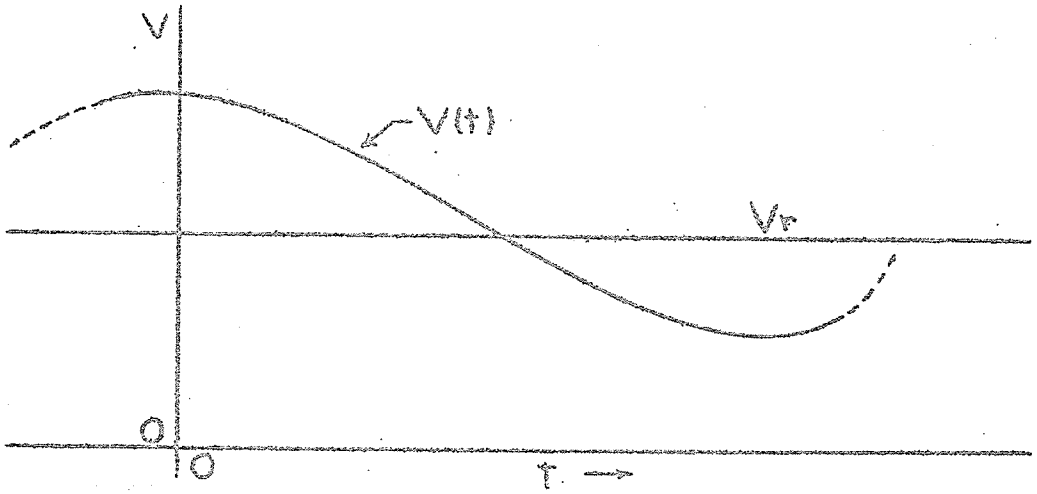

Figure 31. Chopper inputs.

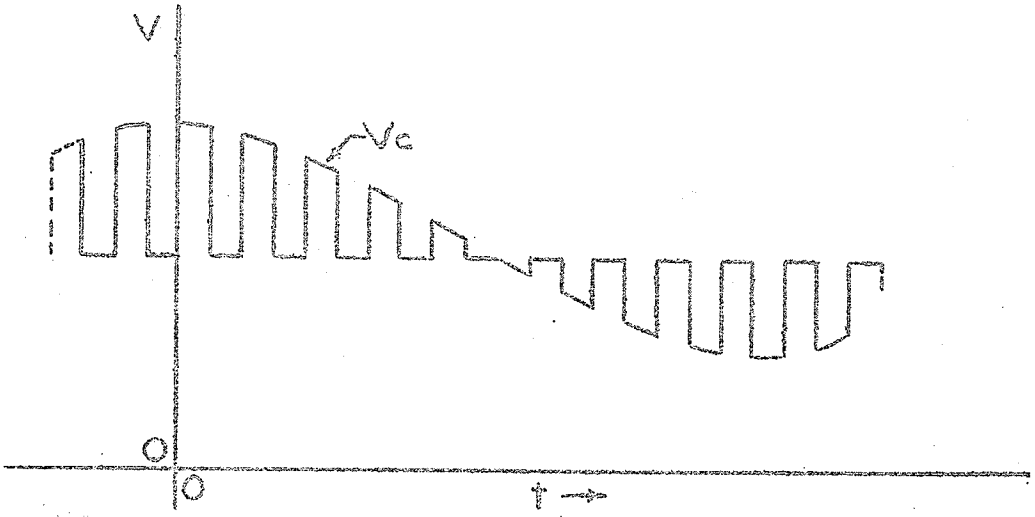

Figure 32. Chopper output.

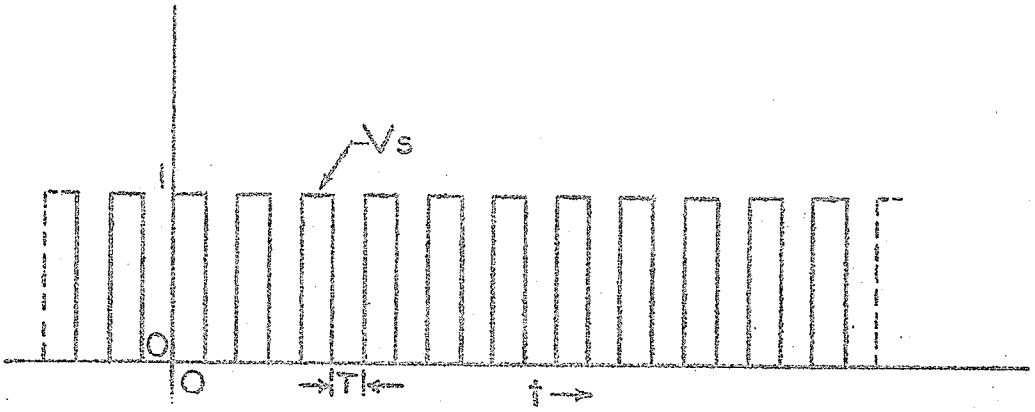

Figure 33. Train of square waves.

by a function consisting of a train of square waves, Vs, shown in Figure 33, and then adding Vr. That is,

$$Vc = (V(t) - Vr)\ Vs + Vr \qquad (13)$$

Since the train of square waves has the Fourier series

$$Vs = \frac{1}{2} + \sum_{n=1,3,5\cdots} \frac{1}{n} \sin n w_o t$$

equation (13) becomes

$$Vc = \left[V(t) - Vr\right]\left[\frac{1}{2} + \sum_{n=1,3,5\cdots} \frac{1}{n} \sin n w_o t\right] + Vr$$

For convenience, let us define $V(t) - Vr$ as the error voltage Ve. Then

$$Vc = Ve\left[\frac{1}{2} + \sum_{n=1,3,5\cdots} \frac{1}{n} \sin n w_o t\right] + Vr$$

$$= \frac{Ve}{2} + Ve \sum_{n=1,3,5\cdots} \frac{1}{n} \sin n w_o t + Vr$$

$$Vc = \frac{Ve}{2} + Ve \sin w_o t + Ve \sum_{n=3,5,7\cdots} \frac{1}{n} \sin n w_o t + Vr \qquad (14)$$

If everything is eliminated from equation (14) but the second term, we are left with Vf, where

$$Vf = Ve \sin w_o t$$

This has the form shown in Figure 34. By means of a detector, the modulation envelope may be removed and used to trigger the

pen-dropping circuit whenever the envelope goes to zero. It is at this point that the difference between V(t) and Vr is zero. As was previously mentioned, the same type of null is obtained (for a given detector) regardless of the polarity through which V(t) approaches Vr.

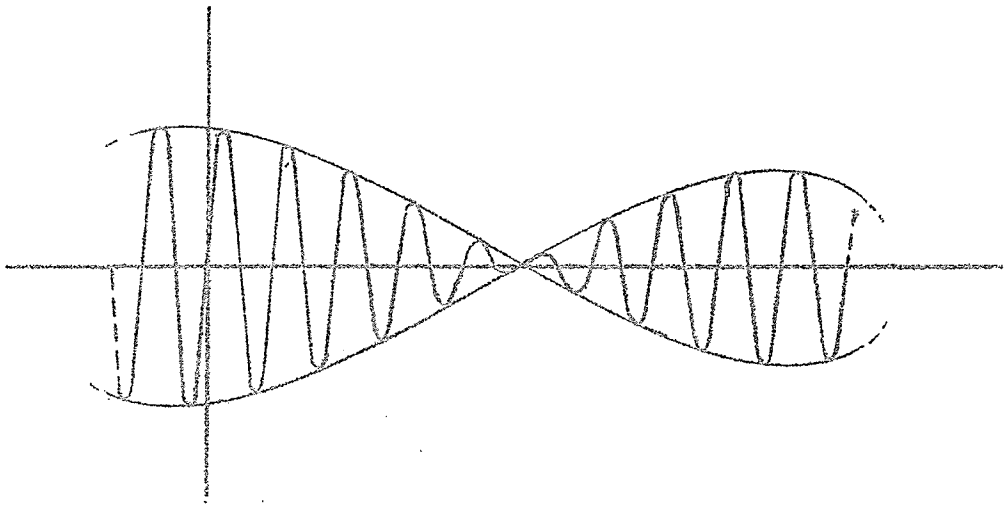

Figure 34. A plot of Ve sin $w_o t$.

Considering equation (14), a method must be found for eliminating all but the second term. This is most easily accomplished by considering the frequency spectrum of V(t) or Ve which will be identical except for a d-c component. In particular, consider w_1 as being the highest significant frequency component of Ve and being of the form cos $w_1 t$. Replacing Ve by cos $w_1 t$ in equation (14)

$$Ve = \frac{1}{2}\cos w_1 t + \cos w_1 t \sin w_o t + \cos w_1 t \frac{1}{3}\sin 3w_o t + \cos w_1 t \sum_{n=5,7\ldots}^{\infty} \frac{1}{n}\sin n w_o t$$

or

$$Vc = \frac{1}{2}\cos w_1 t + \frac{1}{2}\left[\sin(w_o+w_1)t + \sin(w_o-w_1)t\right] +$$

$$\frac{1}{6}\left[\sin(3w_o+w_1)t + \sin(3w_o-w_1)t\right] + \text{higher frequency terms} \quad (15)$$

The line frequency spectrum of equation (15) is given in Figure 35. A consideration of the lower frequency components of Ve will yield similar line spectra with frequency components included within the shaded regions of Figure 36.

By passing the chopper output, Vc, through an ideal band-pass filter of centre frequency w_o and bandwidth $2w_1$ (where w_1 is the highest significant frequency component of Ve) everything will be removed except frequency components in the range $w_o - w_1$ to $w_o + w_1$. These are simply those frequencies arising from the term Ve sin $w_o t$ in equation (2). In order to avoid delay distortion the filter must also have a linear phase shift characteristic. Thus a method of obtaining balanced modulation of Ve has been found.

For an ideal filter, w_o must be greater than, or equal to, $2w_1$. However, an ideal filter is not obtainable, and in the comparator, a tuned amplifier consisting of a difference amplifier with a twin-T filter in a feedback loop was employed. In this case w_o is about 100 times the highest anticipated frequency component of V(t). One other aspect of the filtering process must be considered however, and this is the discontinuity of 180 degrees in the phase shift characteristic of the twin-T filter at the null frequency. For this reason the

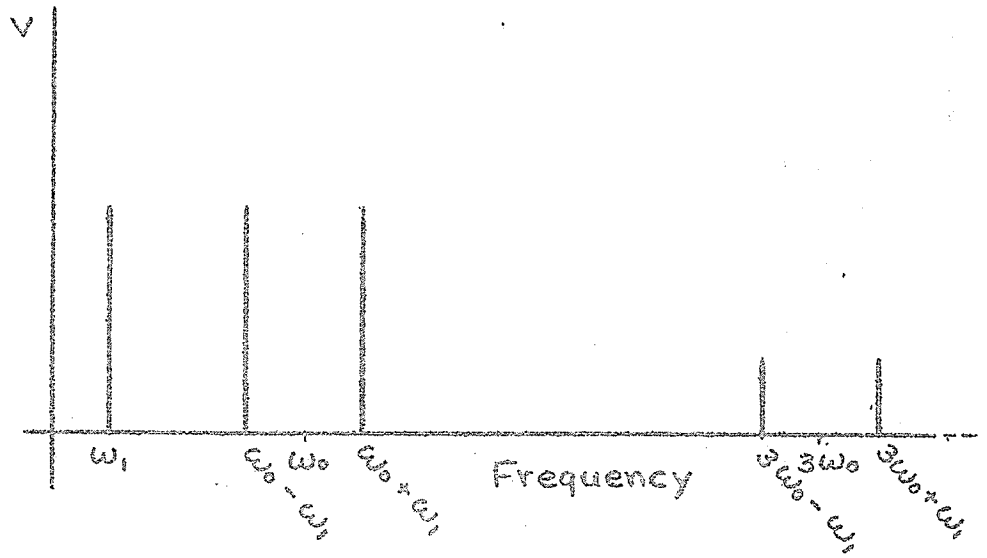

Figure 35. Frequency spectrum of equation 15.

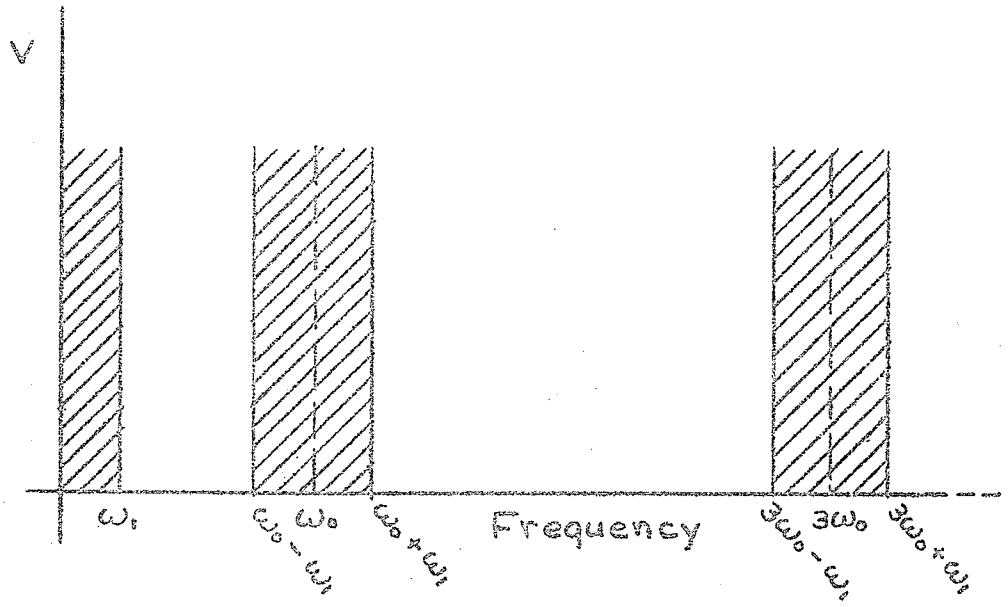

Figure 36. Frequency range of equation 14.

chopper frequency, w_o, was adjusted to be slightly above the null frequency of the twin-T, yet still within the pass-band of the tuned amplifier.

An illustration of the effectiveness of the system is given in Figures 37 and 38 which are oscillograms of the chopper output and tuned-amplifier output respectively for a co-sinusoidal input of 4-cps. The chopping frequency is 400-cps.

This type of comparator has several advantages over conventional types, including:

1. Drift free operation.
2. High sensitivity or resolution.
3. Operation regardless of the polarity through which the reference voltage is approached.

Such a system may be used at high frequencies by using an electronic modulator. Unfortunately, some sensitivity will be sacrificed since electronic modulators are inherently noisier than choppers. By further amplification, using R-C coupled or tuned amplifiers, the resolution of the system may be greatly improved.

A simple diode detector removes the modulation envelope which will have very sharp positive or negative going spikes (depending on the diode orientation) as V(t) approaches Vr. In the comparator under discussion, detection is followed by two stages of d-c amplification before the signal is applied

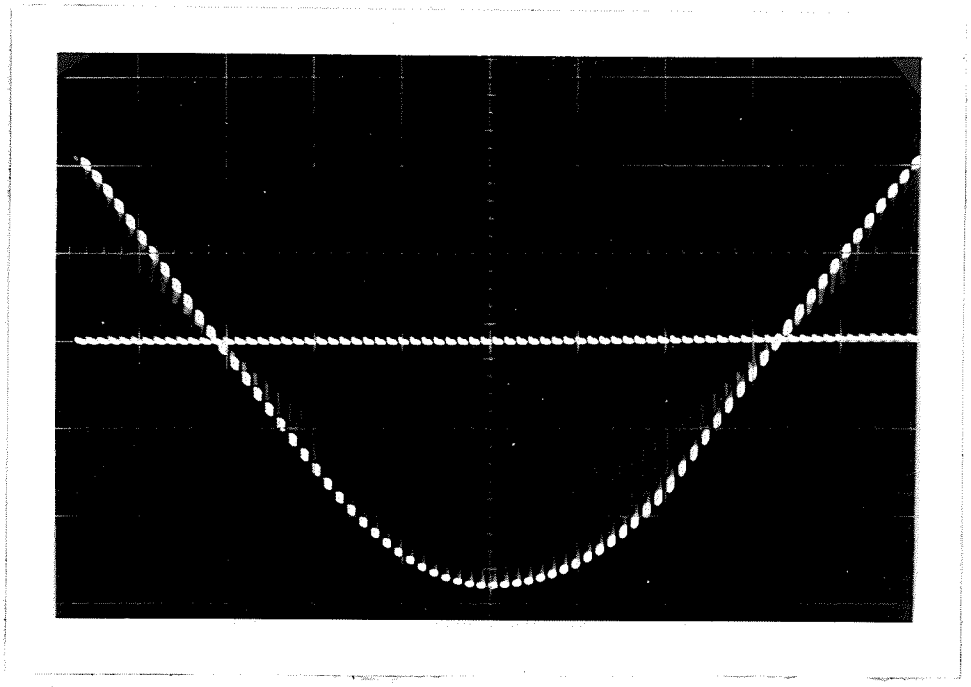

Vert.scale:
.5V/div.

Hor.scale:
20 msec./div.

Figure 37. Chopper output.

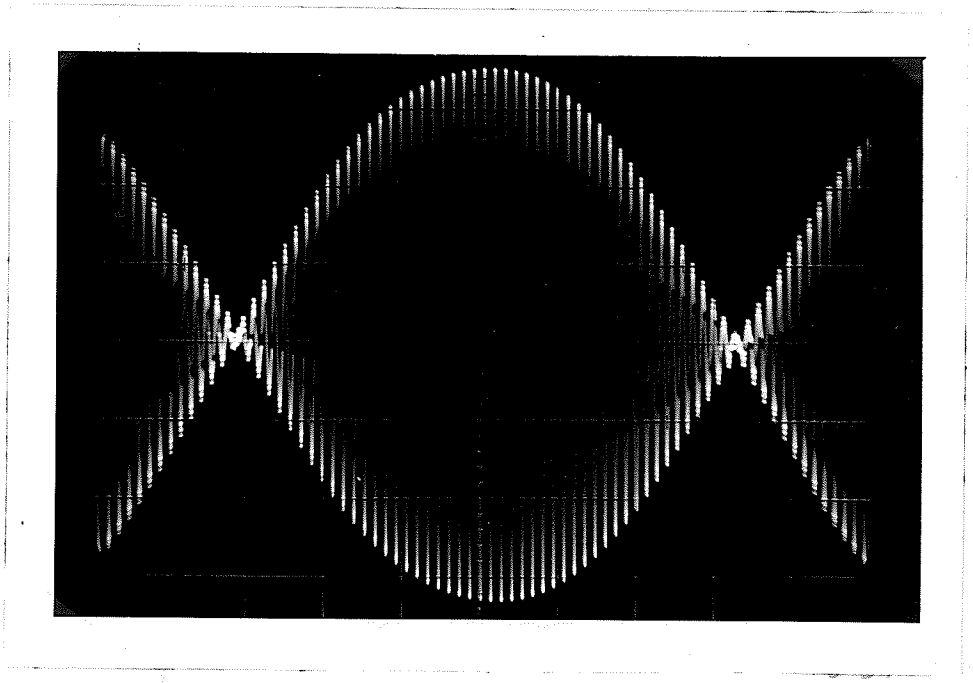

Vert.scale:
2V/div.

Hor.scale:
20msec./div.

Figure 38. Tuned-amplifier output.

to the pen-dropping circuit. Drift is of little consequence at this point because of the relatively high level of the detector output. However, as a precaution the first d-c stage is a difference amplifier.

II. THE PEN-DROPPING CIRCUIT

The pen-dropping circuit is similar in nature to the line-type modulator commonly employed in radar transmitters. A thyratron switch is used, while the pen-dropping relay coil replaces the pulse transformer and an electrolytic capacitor replaces the pulse-forming network. This is shown schematically in Figure 39.

Assuming capacitor C to be fully charged, the thyratron will fire whenever the grid potential rises to a sufficiently high value. This allows C to discharge through the relay coil causing the pen to drop momentarily. As C discharges, plate current through the thyratron drops, and deionization follows.

The capacity of C and the voltage to which it is charged determine the length of time the pen relay remains activated. On a basis of 90 volts, C was chosen to be 100 microfarads by cut and try methods.

Capacitor C is recharged through resistor R and two voltage-regulator tubes (OB2's), the purpose of the latter being to allow C to charge to only 90 volts. (This voltage requirement was dictated by the voltage rating of a damping diode connected across the pen-dropping relay coil, both

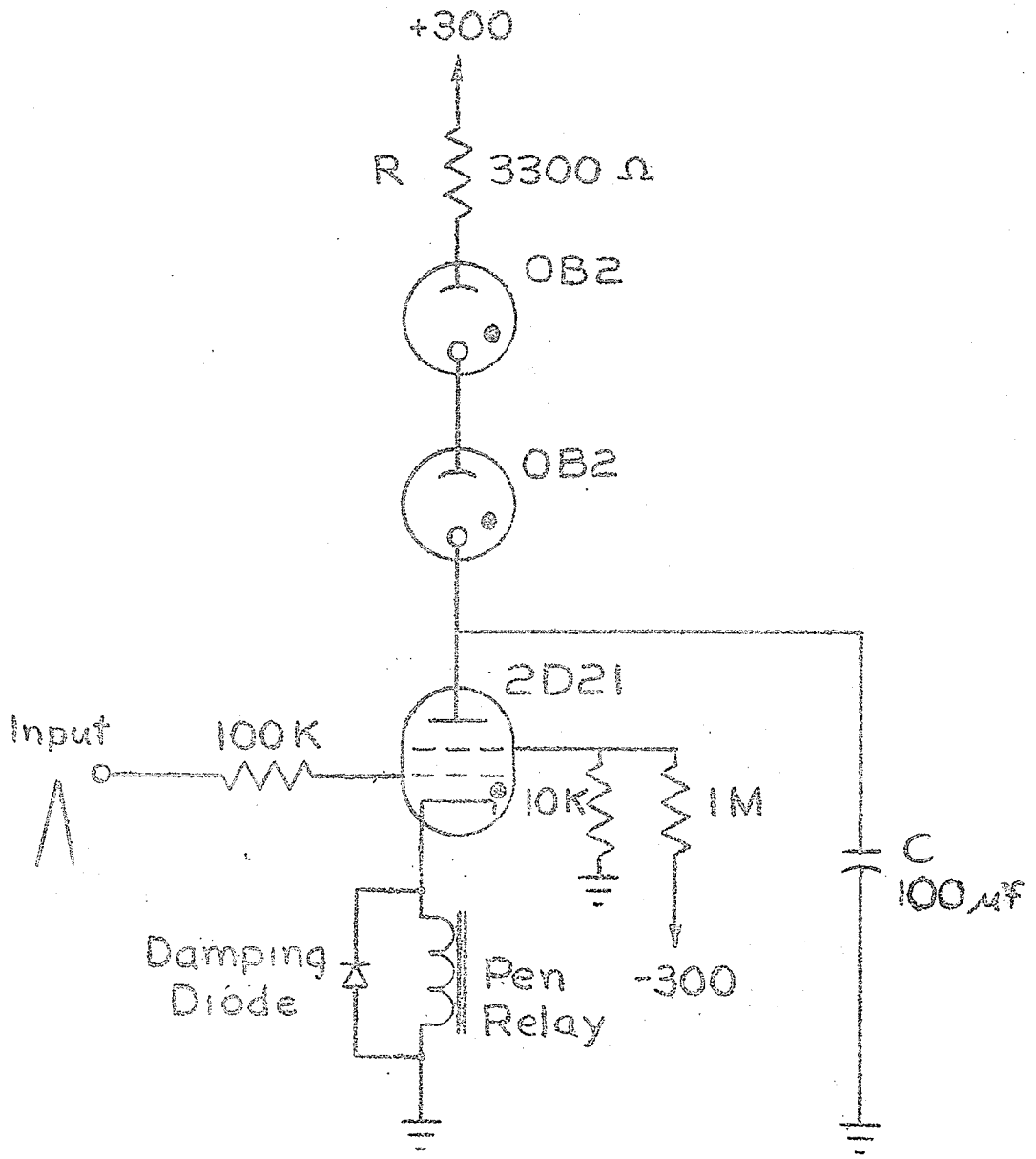

Figure 39. Pen-dropping circuit.

being integral parts of the X - Y recorder.) Resistor R was chosen for minimum charging time while still allowing the thyratron current to fall to the deionization level.

No information is available as to the life expectancy of the 2D21 thyratron under high peak current conditions. However, no trouble has been experienced after about 1000 operations.

The Variable-Reference Limiter

Another unconventional circuit is the variable-reference limiter, designed to ensure long chopper contact life. The voltage between chopper contacts is limited to two volts by what is essentially a parallel-diode limiter whose limiting levels are Er + 2 and Er - 2 (where Er is the reference voltage applied to one of the chopper contacts). Since Er may be set to different values the limiting levels must be able to follow Er. This is accomplished by the circuit of Figure 40.

This circuit consists of a cathode follower operating at two volts bias (when Er = 0) which may be set by the screen resistor, R_1. A zener diode in the cathode circuit operates in the zener region, and provides a constant voltage drop of four volts as indicated in Figure 40. With this arrangement, the limiting diodes, d_1 and d_2, may be returned to potentials two volts above and below the reference voltage.

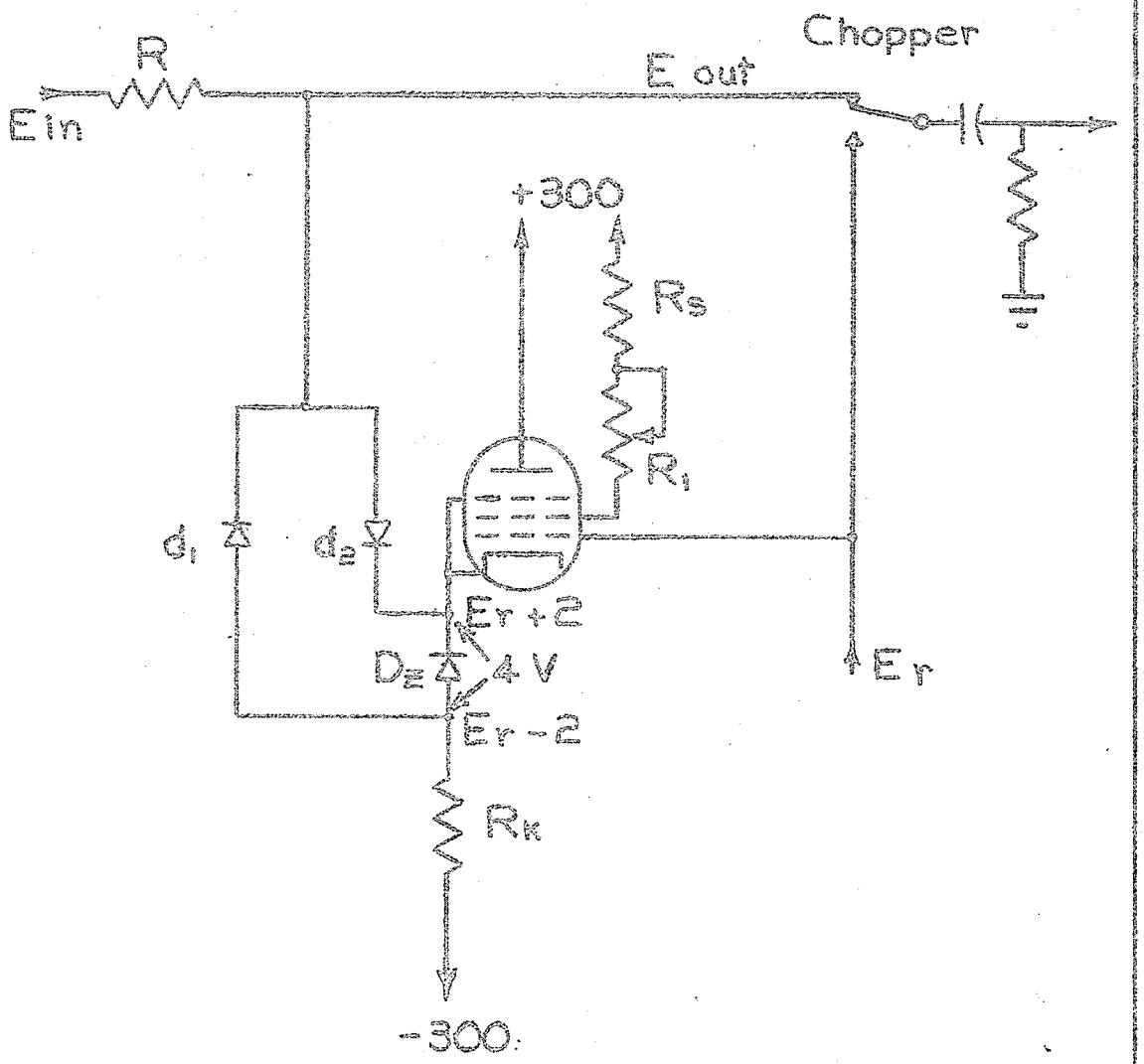

Figure 40. Variable - reference limiter.

If Er - 2 < Ein < Er + 2 (where Ein is the input voltage) then the limiting diodes will be reverse biased, and the equivalent input circuit will be as shown in Figure 41.

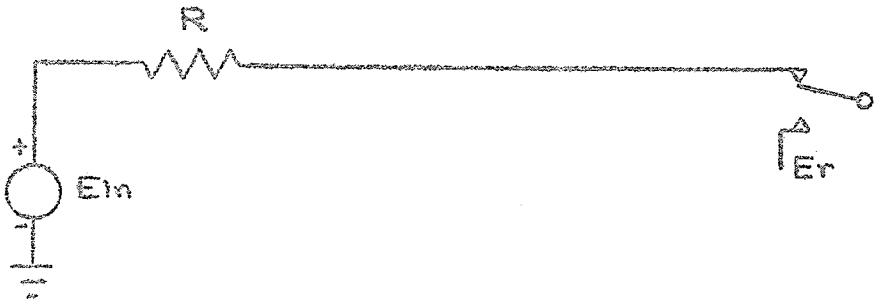

Figure 41. Equivalent chopper-input circuit for

Er - 2 < Ein < Er + 2

If Er + 2 < Ein < Er - 2 then the equivalent input circuit will be as shown in Figure 42.

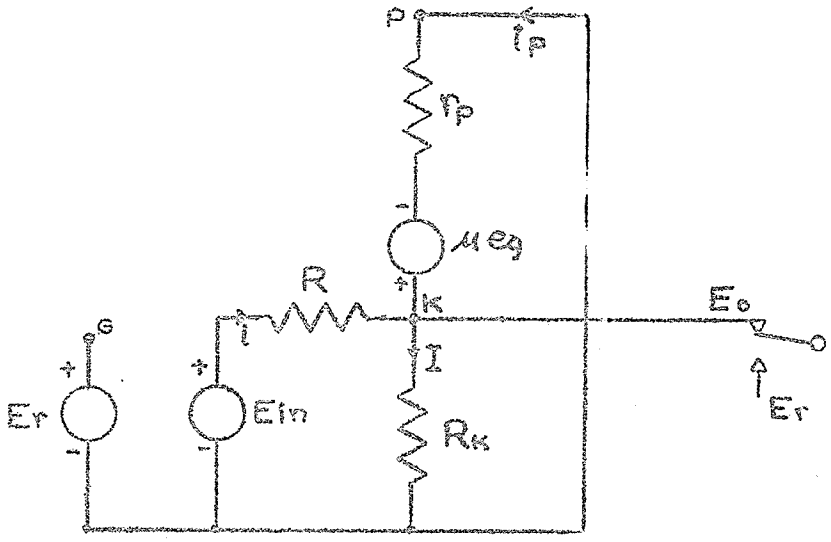

Figure 42. Equivalent chopper-input circuit for

Er + 2 < Ein < Er - 2

From the equivalent circuit:

$$Eo = I R_k \qquad i_p = \frac{\mu eg - Eo}{r_p}$$

$$eg = Er - Eo \qquad I = i + i_p$$

$$i = \frac{Ein - Eo}{R} = \frac{Ein}{R} - \frac{Eo}{R}$$

From the flow graph analysis (Figure 43)

$$Eo = \left[\frac{Ein\ R_k}{R} + \frac{Er\mu R_k}{r_p}\right]\left[\frac{r_p R}{r_p R + R_k r_p + R_k R(\mu + 1)}\right]$$

$$= \frac{Ein\ R_k}{R + R_k + \frac{R_k R(\mu + 1)}{r_p}} + \frac{Er\mu R_k R}{r_p\left[R + R_k + \frac{R_k R(\mu + 1)}{r_p}\right]}$$

If it is assumed that

$$\frac{R_k R(\mu + 1)}{r_p} >> R + R_k$$

then

$$Eo \approx \frac{Ein}{\frac{R}{r_p}(\mu + 1)} + \frac{\mu Er}{(\mu + 1)}$$

and if $\mu >> 1$

$$Eo \approx \frac{Ein}{R\ gm} + Er$$

The term $\frac{Ein}{Rgm}$ must be minimized since it represents that part of the contact voltage, Eo, above Er. This can be accomplished by making R large and by choosing a tube with a large gm. In the present circuit a 6AU6 was used which had a gm of 1000 μmhos and a r_p of 500 kilohms at the operating point, (these are approximate values only).

Setting up the flow-graph of Figure 42 gives

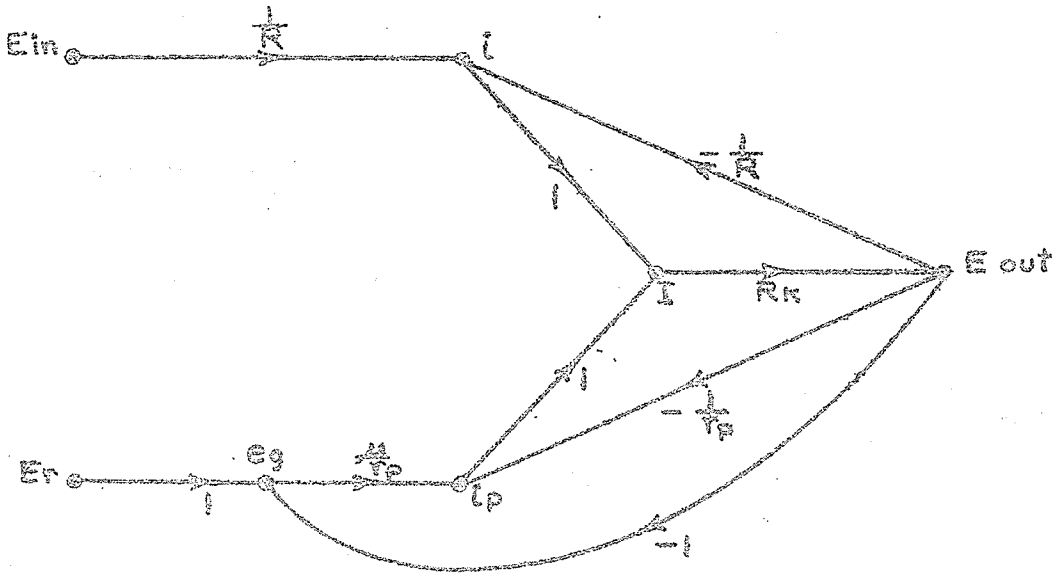

which may be simplified, by eliminating node eg, to yield

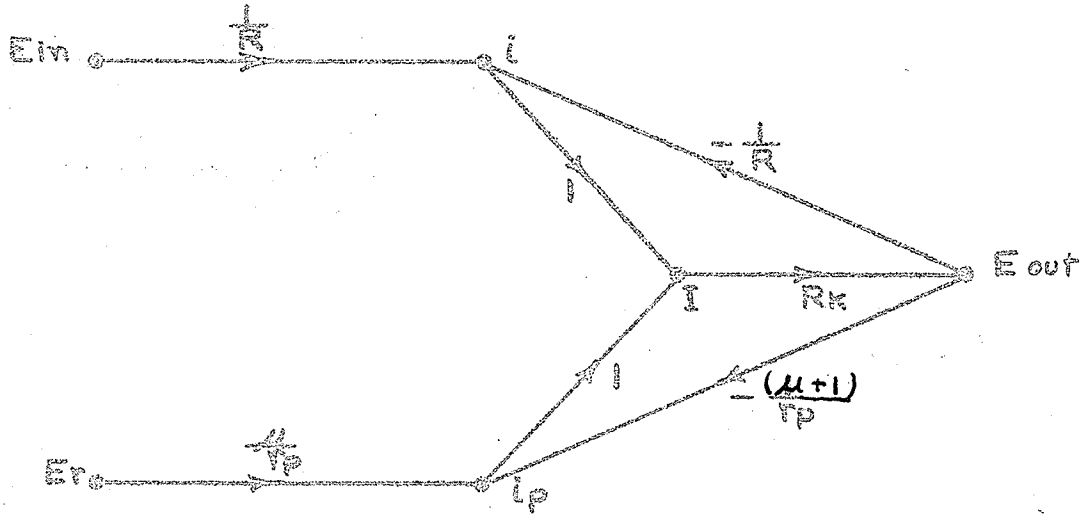

Figure 43a. Flow-graph analysis of the limiter.

Eliminating nodes i and i_p gives

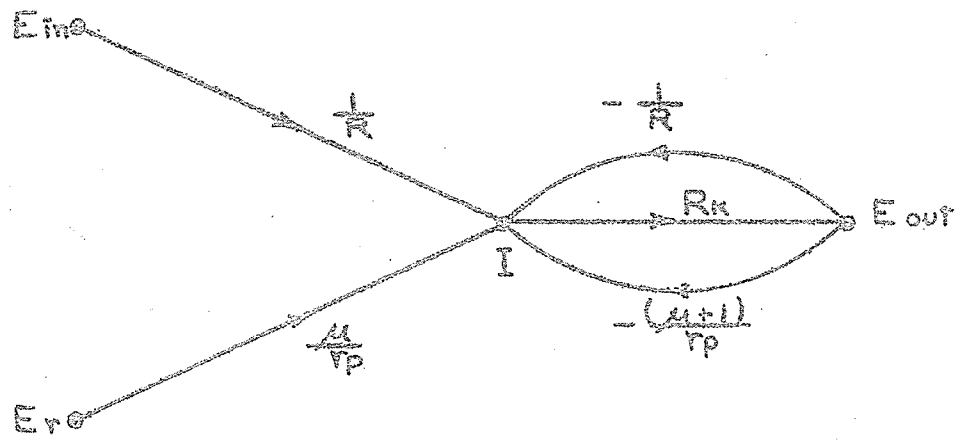

which may be further simplified to

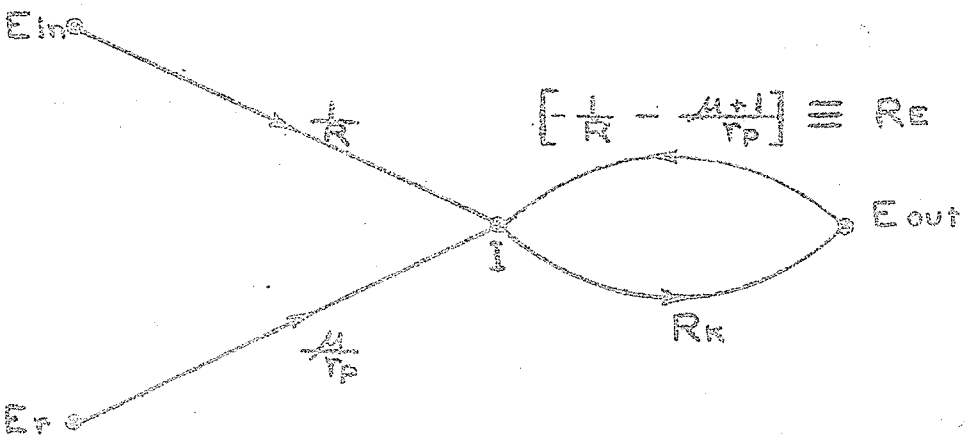

Figure 43b. Flow-graph analysis of the limiter.

Eliminating node I yields

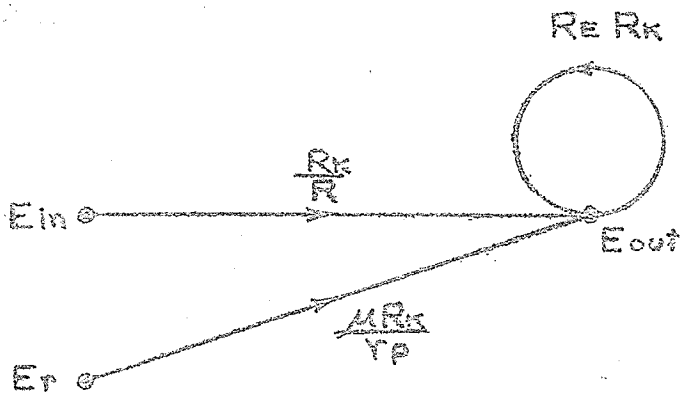

to which the feedback theorem may be applied to give

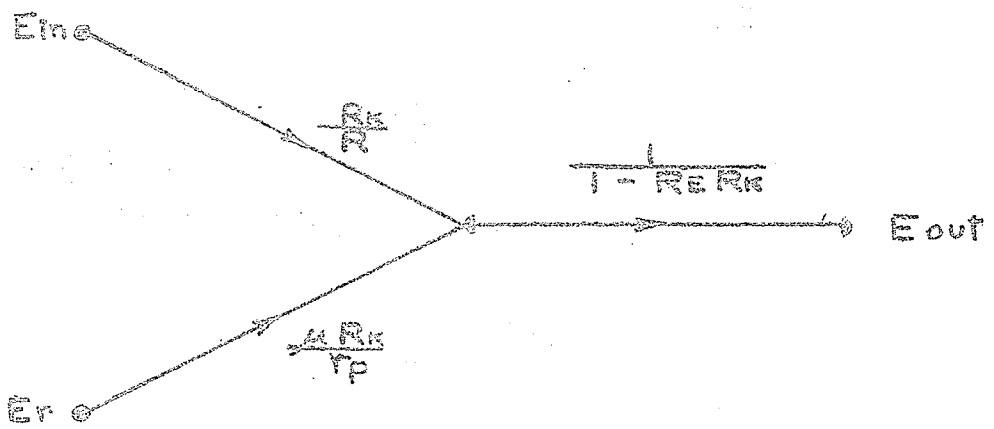

The final result is:

$$E_{out} = \left[\frac{E_{in} R_K}{R} + E_r \frac{\mu R_K}{r_p}\right] \left[\frac{R r_p}{R r_p + R_K r_p + R_K R(\mu+1)}\right]$$

Figure 43c. Flow-graph analysis of the limiter.

It may be noted that the gain of the cathode follower is less than one. In the region where d_1 and d_2 are reverse biased, the gain, G, is given by

$$G = \frac{\mu R_k}{r_p + (\mu + 1)}$$

Thus, a two volt bias cannot always be maintained, although this is of no consequence provided the bias change does not exceed certain limits. For example, it may be assumed that the tube is operating at its normal bias level of two volts with Er = 0. If Er swings to -45 volts and the cathode potential only changes by 42 volts, due to a relatively low gain, then the cathode potential is

$$2 - 42 = -40 \text{ volts.}$$

The lower end of the zener diode will be at a potential of -44 volts. In this case, limiting action will take place before Ein reaches -45 volts. However, if proper operation of the comparator is to be maintained, then limiting must not take place until Ein $<$ -45 volts. In order to satisfy this requirement the following condition must hold:

$$|Er - GEr| < bo$$

where bo is the bias level when Er = 0. The circuit of Figure 41 provides satisfactory operation for Er between plus and minus 50 volts.

Since the cathode follower gain is less than unity and the limiting action imperfect, it is possible for the potential between chopper contacts to exceed the previously specified value of 2 volts. Nevertheless, the limiter provides a large amount of protection for the chopper.

APPENDIX II

ADJUSTMENT OF REFERENCE PHASORS

The four reference phasors of the pole-zero machine ($6\angle 0^\circ$, $6\angle 90^\circ$, $6\angle 180^\circ$ and $6\angle 270^\circ$), produced by the reference oscillator, must be adjusted so that they are equal in magnitude and separated by exactly 90 degrees in phase.

A preliminary adjustment involves making the magnitudes nearly equal by adjusting each phasor to be 6 volts rms, as observed on a high precision a-c voltmeter.

Opposite phasors, for example $6\angle 0^\circ$ and $6\angle 180^\circ$, are then adjusted to be equal in magnitude and 180 degrees apart in phase. This is accomplished by first connecting the two phasor outputs to opposite ends of a centre-tapped resistor. An a-c voltmeter connected to this centre tap indicates the resultant of the two phasors; therefore, they may be made equal and opposite by adjusting for a null on the voltmeter. In the pole-zero machine, an accurately centre-tapped resistor and a sensitive voltmeter allow the magnitudes to be made equal within about 3 millivolts and the phase to be accurate within about .03 degrees. The above process is repeated for $6\angle 90^\circ$ and $6\angle 270^\circ$.

The construction of the reference oscillator is such that the angle between $6\angle 0^\circ$ and $6\angle 90^\circ$ may be varied without

seriously affecting the previous adjustments. With the phasors as shown in Figure 44, the proper phase relationships may be obtained by adjusting the angle of $6\angle 90^{\circ}$ (and consequently $6\angle 270^{\circ}$) so that Va = Vb . This may be accomplished with the circuit shown in Figure 45 connected as indicated. Providing the components are matched, the d-c voltmeter reads the difference between the peak values of Va and Vb so that the phasors may be set to within a few minutes of their desired positions by adjusting the phase control for a null on the voltmeter.

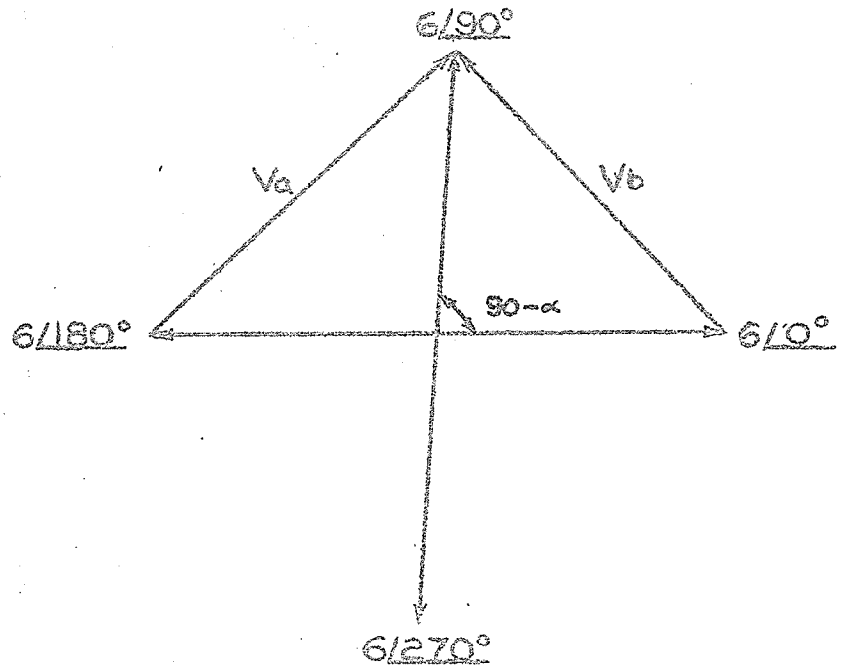

Figure 44. Reference phasors.

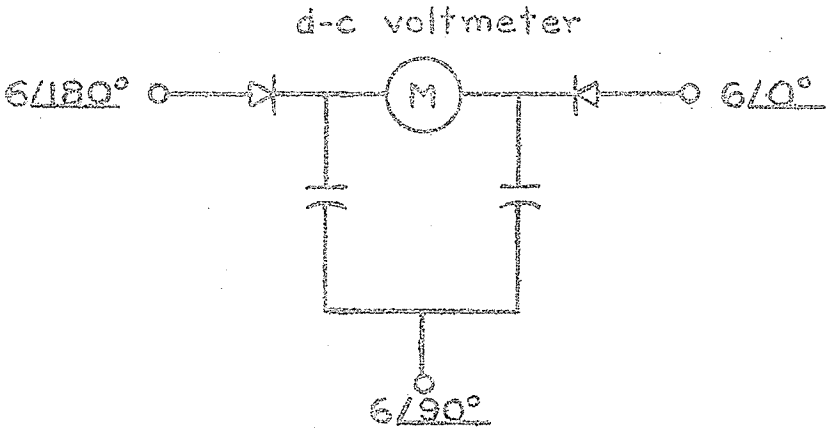

Figure 45. Phase-error indicator.

APPENDIX III

THE ZERO-ORDER HOLD CIRCUIT

The zero-order hold circuit used in the jw-sweep unit, the plan-sweep unit, the error unit, and the output unit, consists basically of a cathode follower with a capacitor, C, connected from grid to ground as shown in Figure 46.

Any voltage applied momentarily (through a gate) to the grid charges the capacitor C which retains this charge when the input is removed. In order to prevent C from discharging rapidly, the input impedance of the cathode follower must be high, that is, grid current must be low. This is accomplished by running the premium 6085 tube at about 80 per cent of its rated filament voltage and making R_k very large (about 1 megohm).

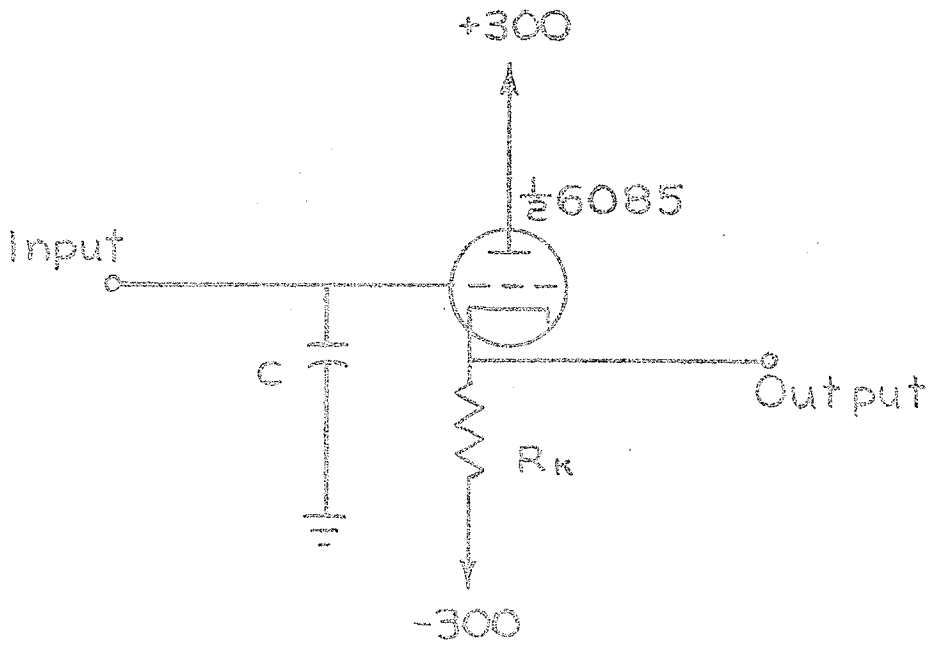

Figure 46. Zero-order hold circuit